LOAD-PATH AND STIFFNESS DEGRADATION OF FLOOR DIAPHRAGMS IN REINFORCED CONCRETE BUILDINGS SUBJECTED TO LATERAL LOADING

PART II: DATA ANALYSIS

Parr, M.[1], Bull, D.[2], Brooke, N.[3], De Francesco, G.[1], Elwood, K. J.[2], Hogan, L.[2], Liu, A.[4], Sullivan, T.[1]

ABSTRACT

An experimental investigation into the degradation of load-paths in damaged diaphragms was conducted to provide answers to the New Zealand structural engineering community following concerns that strut-and-tie load-paths could not cross wide cracks that develop around the floor perimeter during earthquake loading demands. A full-scale super-assembly concrete moment frame specimen with a hollow-core flooring system installed was subjected to realistic drift deformations to induce damage in the floor, followed by in-plane shear deformation demands to assess the ability of the diaphragm to transfer load between frames at different floor damage levels. It was found that compression struts could form across much wider cracks in floors than previously anticipated. This was due to contact compressive stresses forming via loose aggregate that lodged within rugged sinusoidal wide floor cracks. Additionally it was found that diaphragm compression struts can only transfer to the primary lateral load resisting frame through beam plastic hinges acting in minor axis shear following gaps opening between the floor and columns at moderate drift demands. Smooth floor-to-column interfaces did not provide the same residual rubble aggregate binding compressive load path observed in cracks within the floor. The primary driver of diaphragm shear stiffness degradation was found to be torsional softening of the perimeter beams of the floor. This was caused by simultaneous bi-directional demands applied to longitudinal beam bars and a phenomenon known as the bowstring effect applying large torsional demands through the beam-floor continuity reinforcement. The diaphragm strength and rate of shear stiffness degradation was found to be highly reliant on earthquake directionality. A set of generalised equations was developed to describe the rate of diaphragm shear stiffness degradation with respect to magnitude and directionality of drift demands.

Part II of II in this journal series provides analysis of the cause and rate of diaphragm stiffness degradation based on instrument data and visual observations as described in Part I (Parr et al. 2022). Analysis of the formation of residual diaphragm load-paths and the relationship between torsional softening of beams with simultaneous bi-directional demands is also investigated.

1 INTRODUCTION AND OBJECTIVES

Observations of wide cracking around the perimeter of floor diaphragms in concrete moment frame buildings following earthquake shaking have led to concerns that the standard strut-and-tie design method for diaphragms does not accurately represent realistic load-paths in floors after they are damaged. This is because the compressive strut components of these load-paths cannot cross air gaps. This could also invalidate the commonly used rigid diaphragm assumption used in structural models for diaphragm elements linking beam and column elements. A residual load-path was proposed for damaged floors describing the floorplate being wedged with large compressive struts linking columns across the short diagonal once the support frame warped into a rhomboidal shape in plan due to failure of the designed load-path. This effect has been compared to a small picture sitting within a larger picture frame, so it is free to move and twist until the picture frame warps, leading to the term “picture frame effect”. A comparison between classic strut-and-tie load-path and the proposed picture frame effect is displayed in Figure 1.

In Part I of this journal series, experimental observations from two full-scale super-assembly frame experiments of crack patterns and floor damage under lateral loading and plan shear demands provided evidence that compressive struts could cross wider cracks than anticipated. It was proposed that residual contact stress load-paths could develop across wide cracks until the crack width reached approximately the aggregate size used in the concrete mix. This was because aggregate rubble was falling between the rugged interfaces of the cracks leading to binding of the two sides of the crack.

PAPER CLASS & TYPE: GENERAL REFEREED

1 University of Canterbury
2 Holmes Consulting LP
3 Compusoft Engineering
4 BRANZ

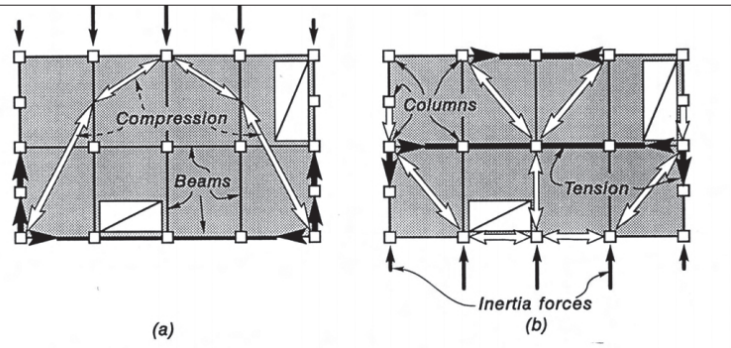

(a) Classic strut-and-tie load-paths (Paulay 1996)

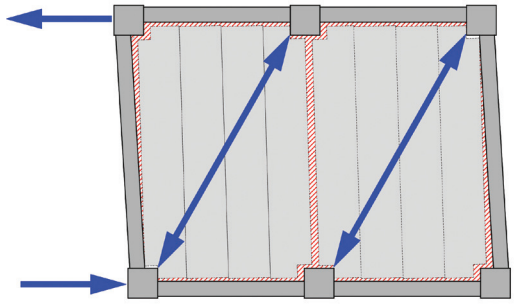

(b) Proposed "Picture Frame effect" (Parr et al. 2022)

Figure 1: Classic strut-and-tie load-paths compared to proposed residual load-path following cracking at floor perimeter

In addition it was found that gaps between the floor and columns developed relatively early (at approximately 1% to 1.5% drift). This meant diaphragm compressive struts could only land within beams from this point on, meaning the proposed "picture frame effect" required some alteration (Parr et al. 2022).

In Part II, analysis of instrumental data from the two super-assembly experiments along with the experimental observations presented in Part I will be used to quantify the degradation rate of the diaphragm plan shear stiffness and identify the primary mechanisms driving diaphragm stiffness degradation.

The layout of the two super assembly experiments is displayed in Figure 2 (a). For simplicity, the first super-assembly experiment will be referred to as TEST 1 and the second will be referred to as TEST 2 as displayed in Figure 2.

When referring to columns or beams, their location on the gridlines will be used. For example, the south-eastern column would be referred to as column A1 and the beam spanning between column A1 and column B1 would be referred to as beam A1B1 (Parr et al. 2022).

Hollow-core units in different positions within the floor system are commonly referred to by different names. The units at the end of the floorplate seated on plastic hinge zones of supporting beams next to longitudinal beams are referred to as alpha units (units 1 and 8 in the 2020 UC super-assembly experiment). Interior units seated on beam plastic hinges are referred to as beta units (units 4 and 5 in the 2020 UC super-assembly experiment). In this paper, units not seated on plastic hinges of the beams (units 2, 3, 6 and 7 in the 2020 UC super-assembly experiment) will be referred to as intra-span units, as they are seated within the span of the supporting beam. Further explanation of terminology related to hollow-core units can be found in (Brooke 2022) (Parr et al. 2022).

TEST 1 used a standard starter bar configuration around the entire floor perimeter, cast-in-place tie bars linking the intermediate beams and a linearised circular loading protocol with 1:1 directionality of loading for the standard loading protocol. The first bay of the specimen had no mesh crossing the beam-floor interface. The second bay did have mesh crossing the beam-floor interface to observe the effects of a stronger connection on the hollow-core units, which had been retrofitted against negative moment failure (Parr et al. 2022).

TEST 2 used different starter bar configurations at the four support ends of the two bays to encourage targeted local hollow-core failure modes to initiate at the critical end. In the first (eastern) bay the northern end of the hollow-core units was designed as the critical end for failure, targeting loss of seating with a weak mesh-only beam-floor interface. In the second (western) bay the southern end of the hollow-core units was designed as the critical end for failure, targeting negative and positive moment failures at the end of the starter bars with high strength beam-floor continuity reinforcement. The targeted critical failure ends of each bay were installed on the diagonals opposite each other to minimise interaction of failure modes that could affect results. Additionally, D12 "stitching" bars were installed linking the two beta units (unit 4 and unit 5) to strengthen the connection after the results from the TEST 1 experiment determined that this was a critical weak point for both the gravity-carrying and diaphragm functions of the floor (Parr et al. 2022).

After the findings detailed in Part I (Parr et al. 2022) and Section 2 related to TEST 1, it was decided that TEST 2 would have a more targeted directionality typical of a pulse or near-fault earthquake shaking. This led to the use of a 1:2 directionality linearised oval protocol as shown in Figure 2 (d). This was considered as the lower bound of likely realistic earthquake directionalities based on research conducted by (Nievas and Sullivan 2017).

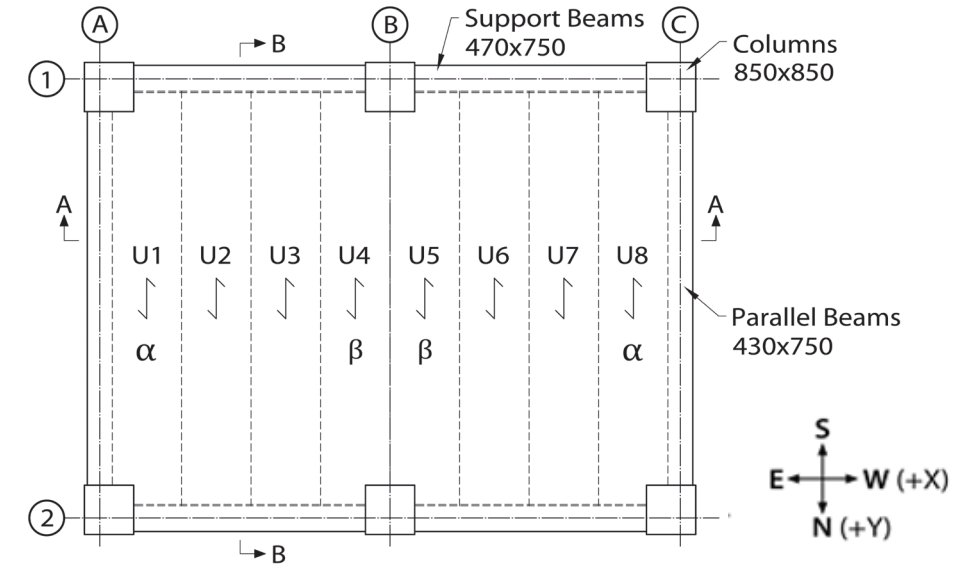

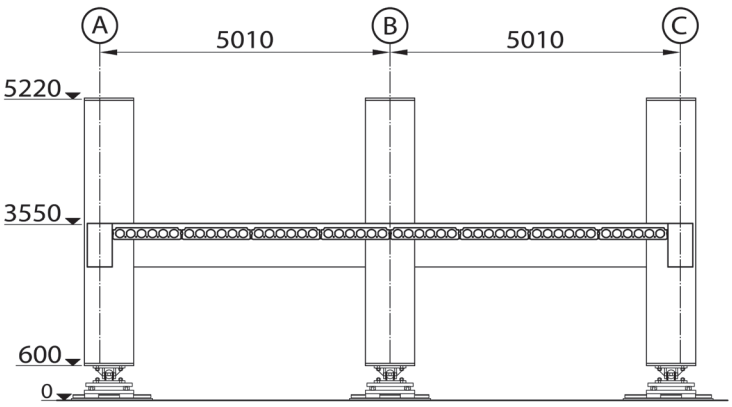

Section B-B

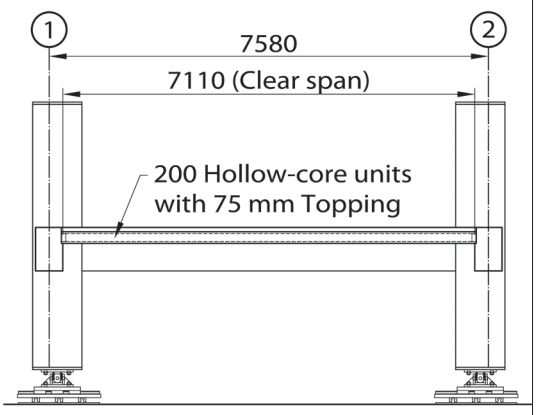

Section A-A

(a) 2020 UC Super-assembly experiment frame layout and nominal dimensions (Büker et al. 2022)

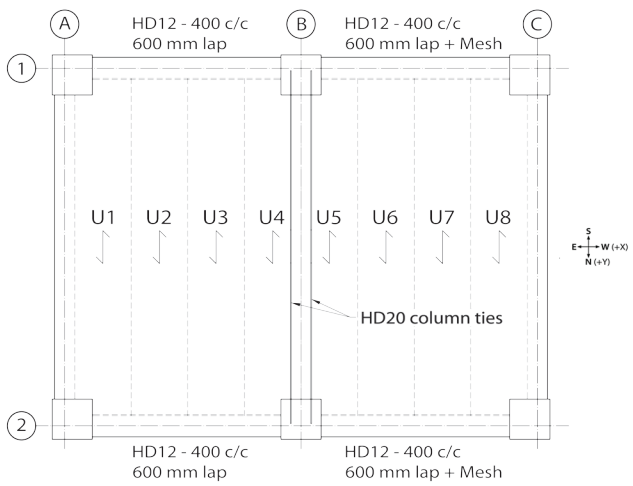

(a) TEST 1 Continuity reinforcement

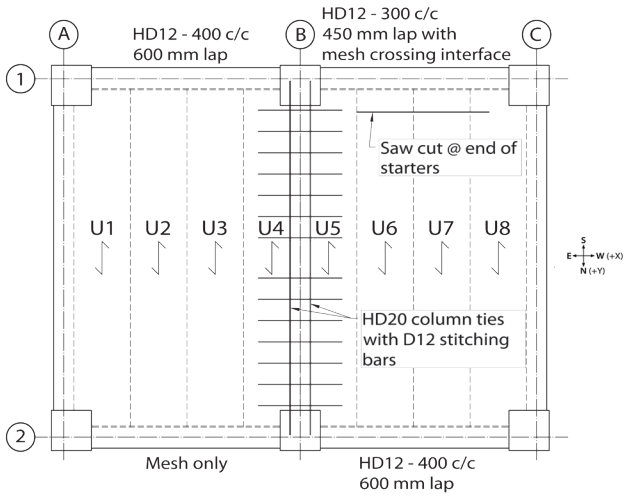

(b) TEST 2 Continuity reinforcement

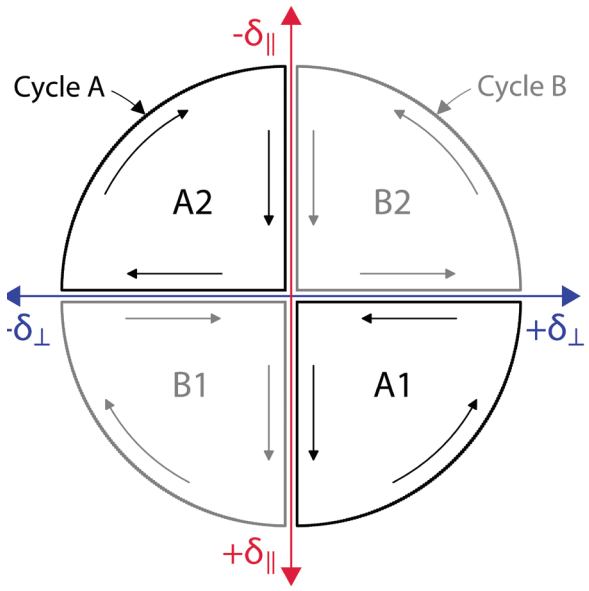

(c) TEST 1 SLP shape

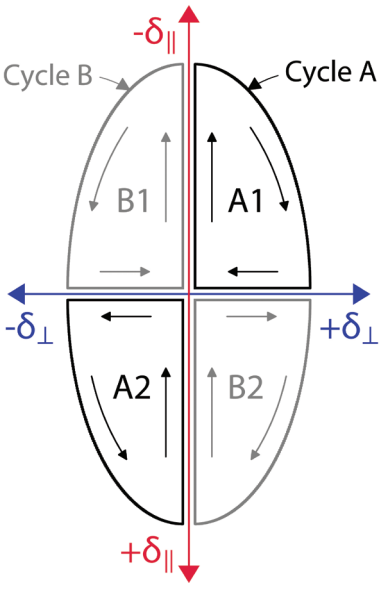

(d) TEST 2 SLP shape

Figure 2: Standard loading protocols and locations of rhomboid loading protocols for the TEST 1 and TEST 2 experiments (Büker et al. 2022)

This meant TEST 1 and TEST 2 would provide an upper and lower bound of simultaneous bi-directional actions imparted into a floor system respectively (Parr et al. 2022).

At different damage states within the floor in each test, the standard loading protocol was stopped to enforce plan shear deformation on the frame (referred to as a rhomboid loading protocol). No drift rotation was applied during the rhomboid loading as the purpose was to isolate the shear stiffness behaviour of the frame and its ability to resist warping via the floor diaphragm. The loading fixity while pushing from strong walls during the rhomboid loading protocols is displayed in Figure 3 and the force/distortion demands of each rhomboid for both tests are displayed in Table 1.

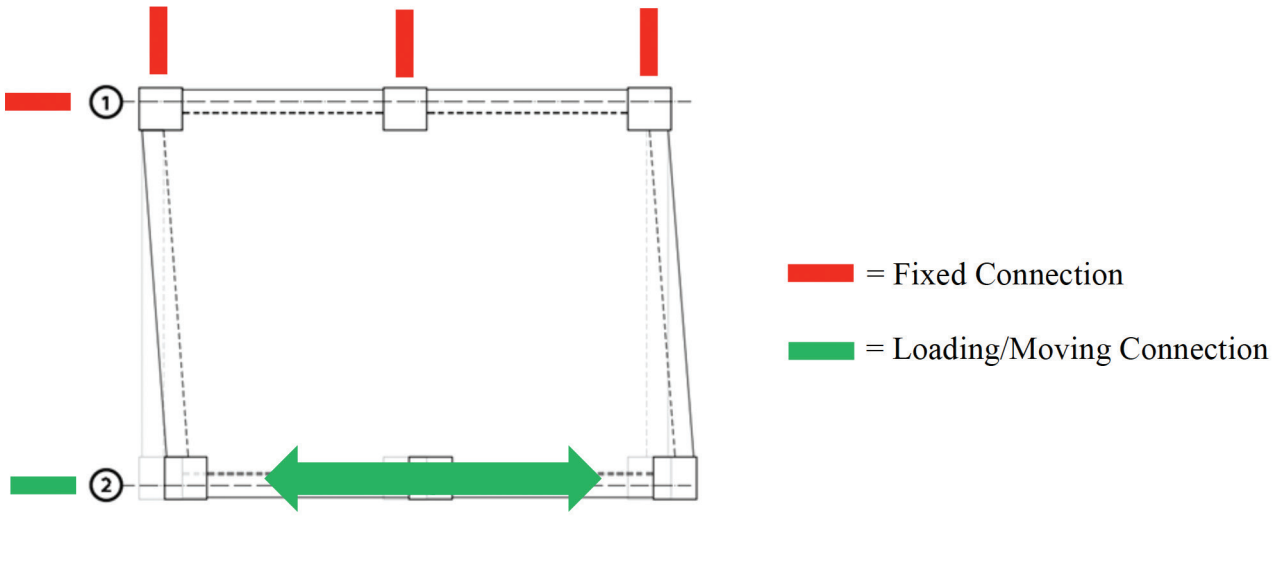

Figure 3: Fixity and loading of the specimen during rhomboid loading (positive shear distortion shown) (Parr et al. 2022)

Table 1: TEST 1 and TEST 2 Rhomboid applied displacement and shear distortion demands

Rhomboid #	+- Plan Shear Distortion, γ (%)				Targeted state of the diaphragm for testing
	Test 1		Test 2		
	± Shear Distortion, γ (%)	± Force (kN)	± Shear Distortion, γ (%)	± Force (kN)	
1	0.01	250	0.005	250	No/low damage to designed load-paths
2	0.05	500	0.02	500	Intermediate damage to design load-paths
3	0.11	450	0.06	600	High damage to designed load-paths
4	n/a	n/a	0.25	700	Extreme damage to designed load paths

Note that the magnitude of each rhomboid loading protocol was different depending on the level of damage the specimen had sustained in previous standard linearised circular loading cycles. This was done to avoid prematurely damaging the specimen before it had softened from the standard loading protocol. Doing so would have lowered the reliability of results from subsequent testing with both the standard loading protocol and rhomboid loading protocols (Parr et al. 2022).

For more detail regarding the super-assembly specimens, loading systems and loading protocols, refer to Part I (Parr et al. 2022) or the thesis (Parr 2022).

The crack maps observed at the end of TEST 1 and TEST 2 are displayed in Figure 4.

Note: The Bowstring Effect

Throughout this paper, a phenomenon known as the "bowstring effect" will be referenced multiple times. The bowstring effect describes the topping steel reinforcement of a diaphragm acting in tension to restrict beam elongation of a concrete moment frame. This creates a balance between the beams attempting to extend acting as a compression arch similar to a bow, and the diaphragm topping reinforcement restricting this by acting in tension similar to a bowstring as discussed in (Lindsay 2004) and (MacPherson 2005).

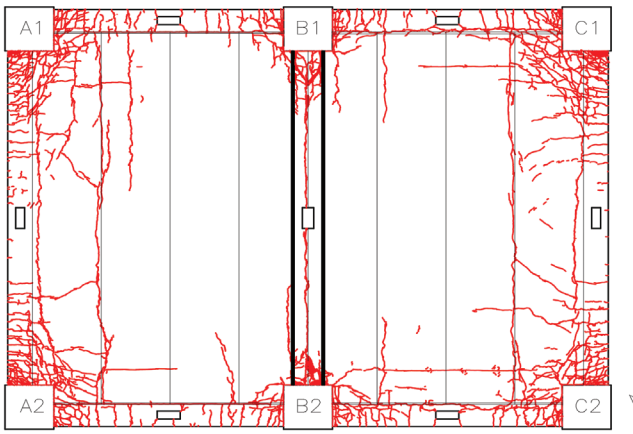

(a) TEST 1 Topping crack map after 3.0% drift

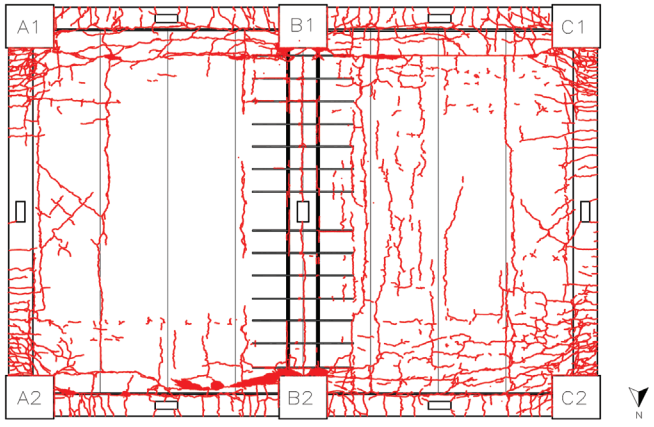

(b) TEST 2 Topping crack map after 5.0% drift

Figure 4: Topping crack maps for TEST 1 and TEST 2 at conclusion of experiments (Parr et al. 2022)

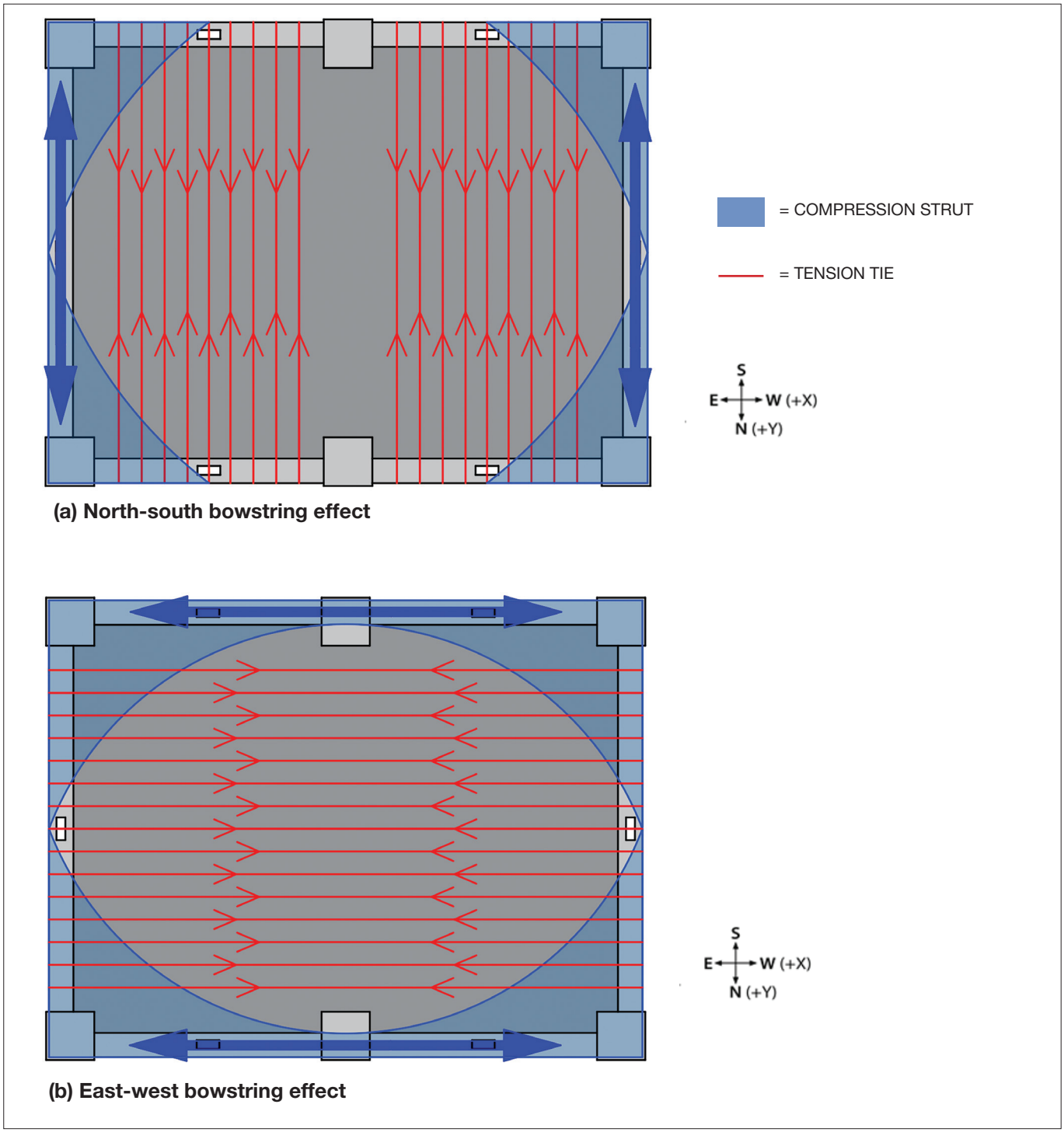

Figure 5: Directionality of the bowstring effect in the 2020 UC super-assembly experiment

If steel reinforcing in the floor topping ruptures this can reduce or even eliminate the restriction to beam elongation provided by the bowstring effect. This is a critical factor in many of the observations relating to residual load-paths discussed in this report.

Throughout the paper there will also be distinction between the bowstring effect acting in different directions across the floor diaphragm. References to a north-south bowstring effect relate to a load-path (for the specimen described in Section 1) like the one displayed in Figure 5 (a). References to an east west bowstring effect relate to a load-path like the one displayed in Figure 5 (b).

2. ANALYSIS OF SUPER-ASSEMBLY TEST RESULTS

2.1 DEGRADATION OF FRAME IN-PLANE SHEAR-MODE STIFFNESS WITH INCREASING DIAPHRAGM DAMAGE

As covered in Section 1, a core objective of the UC 2020 super assembly experiments was to determine how load-paths evolve as a diaphragm degrades during an earthquake. The observations from TEST 1 and TEST 2 provided some unexpected results.

When wide cracks form around the perimeter of a floor in an RC frame structure, the anticipated behaviour was that no compression struts would be able to form across the crack openings between both the floor and columns as well as the floor and beams until rhomboidal deformation of the surrounding frame elements in plan led to binding with the floor. When considering the force displacement response of a structure with shear deformation applied, this would have led to very low stiffness at low shear deformations until binding occurred across the diagonal. This is because the only elements contributing resistance to shear deformation before binding would be the beams orthogonal to the loading direction acting in shear and bending about their weak axis as displayed in Figure 6.

The force displacement response of this anticipated system would have looked like what is displayed in Figure 7. Based on this model, higher damage states with wider cracks would be associated with larger shear deformations in the horizontal plane (in plan) required before jamming

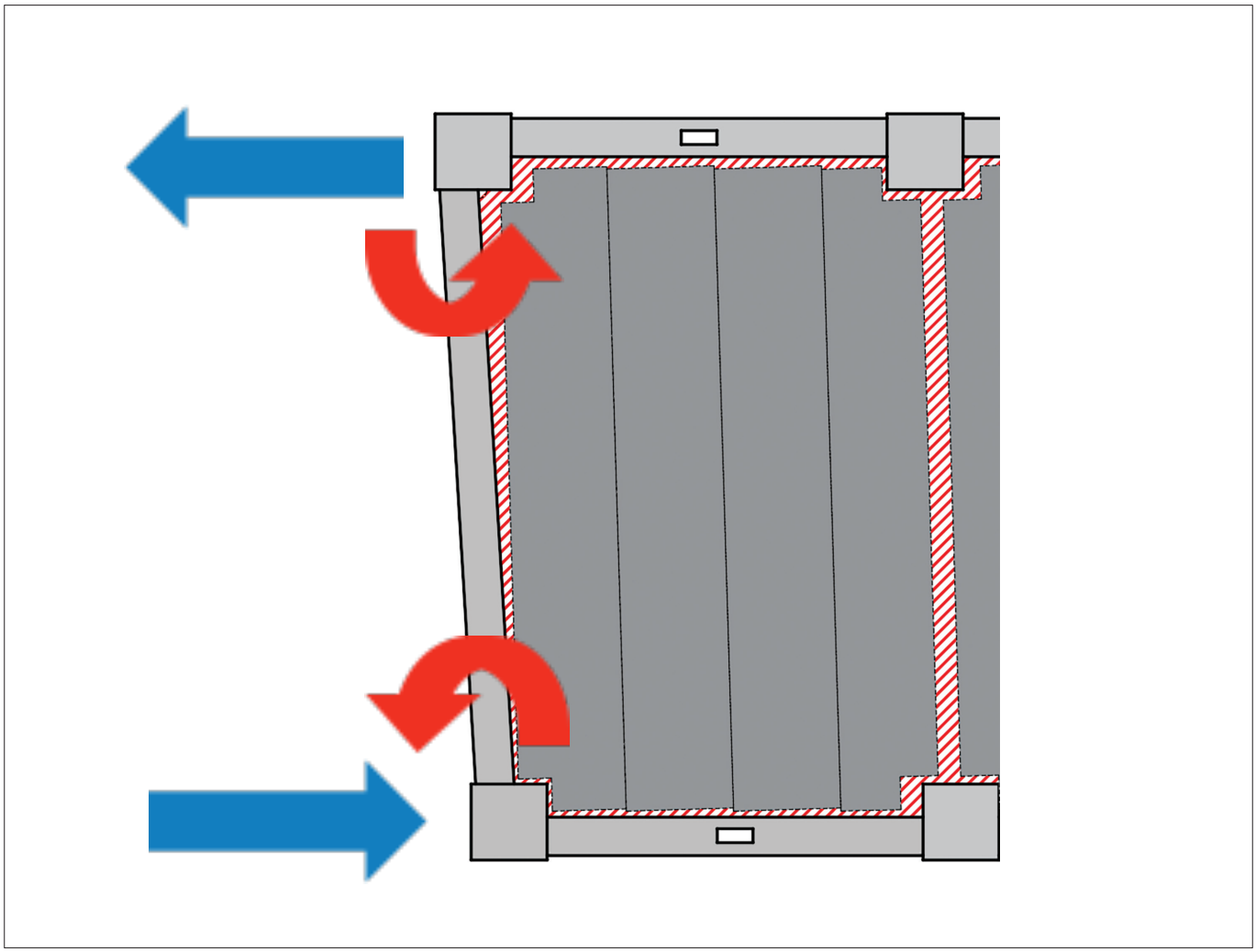

Figure 6: Expected behaviour of the diaphragm and surrounding beams prior to binding across the diagonal with stiffness contribution only provided by longitudinal beams acting in shear/moment about their weak axis

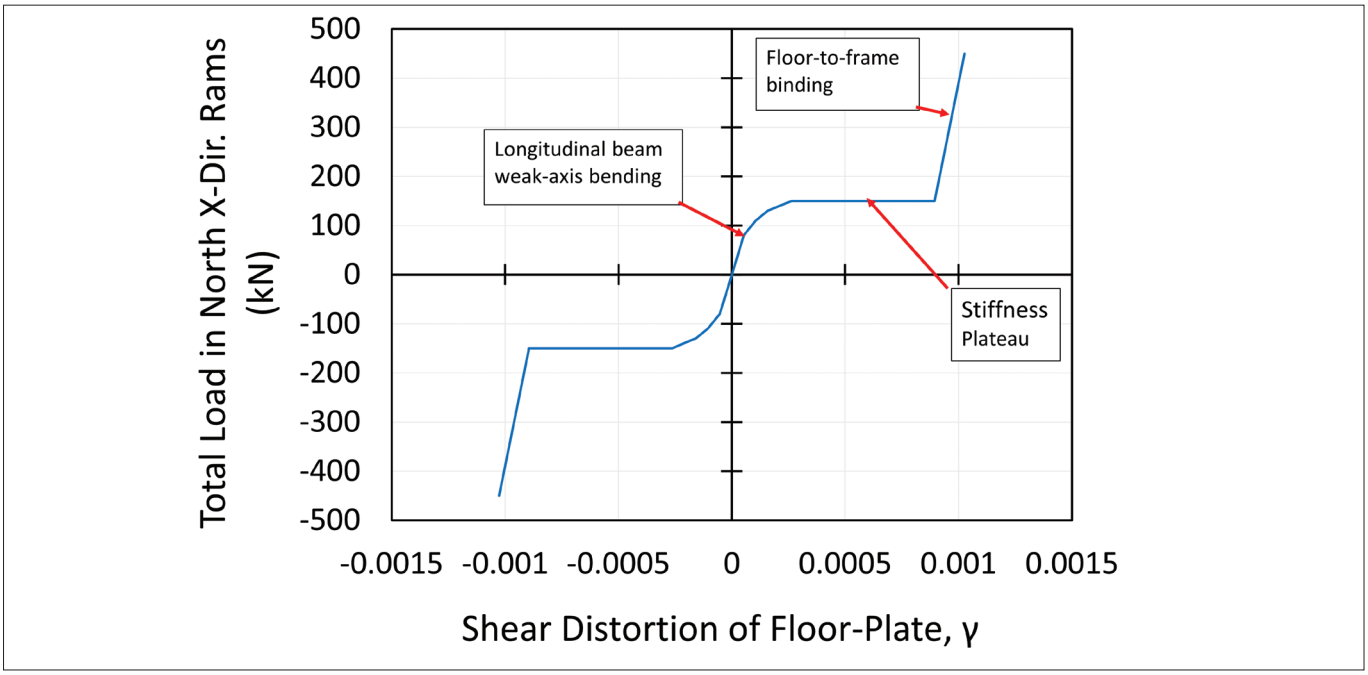

Figure 7: Expected Plan Shear Stiffness Behaviour with the Proposed "Picture Frame Effect"

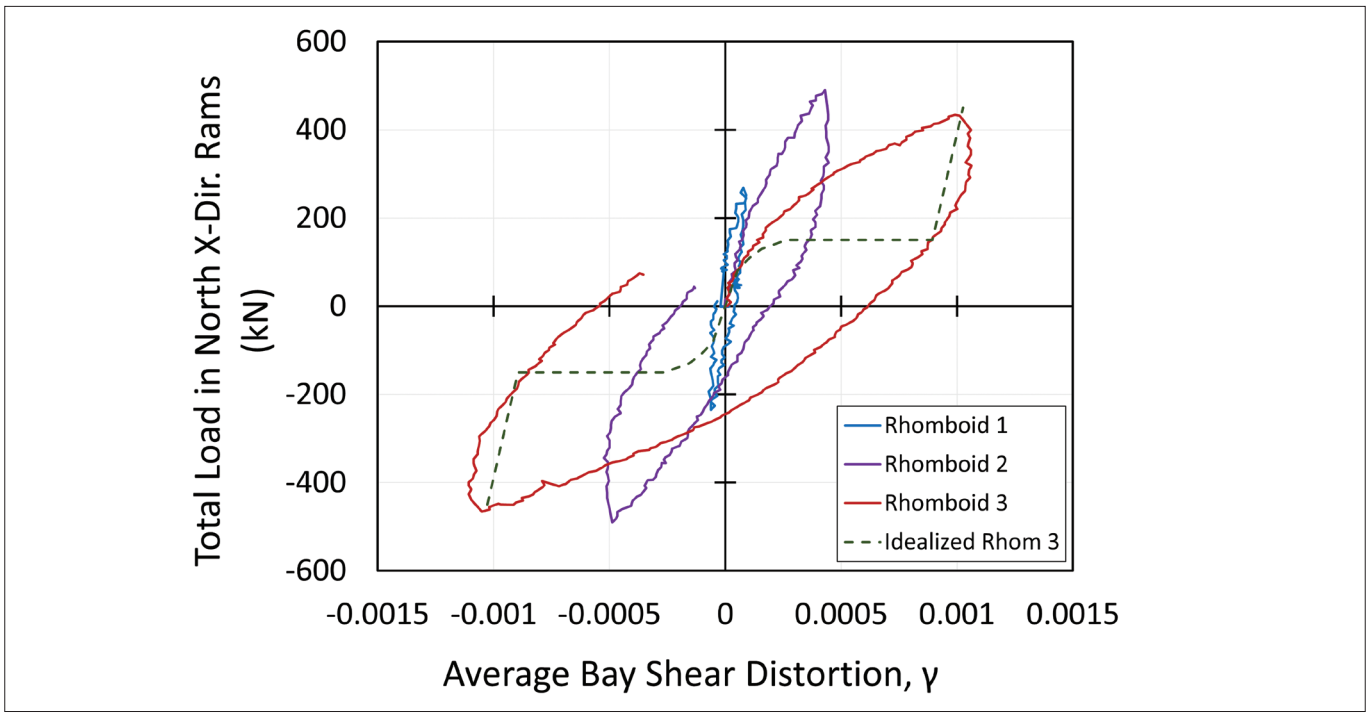

Figure 8: Observed plan shear stiffness behaviour for rhomboid loading protocols undertaken in TEST 1

occurred across the diagonals of the floor. Once jamming occurred, the stiffness would increase greatly.

The true behaviour observed in the 2020 UC super assembly experiments deviated significantly from the anticipated behaviour. The force-distortion behaviour observed in the rhomboid protocols undertaken throughout TEST 1 are displayed in Figure 8.

The force-distortion behaviour observed in the rhomboid protocols undertaken throughout TEST 2 are displayed in Figure 9.

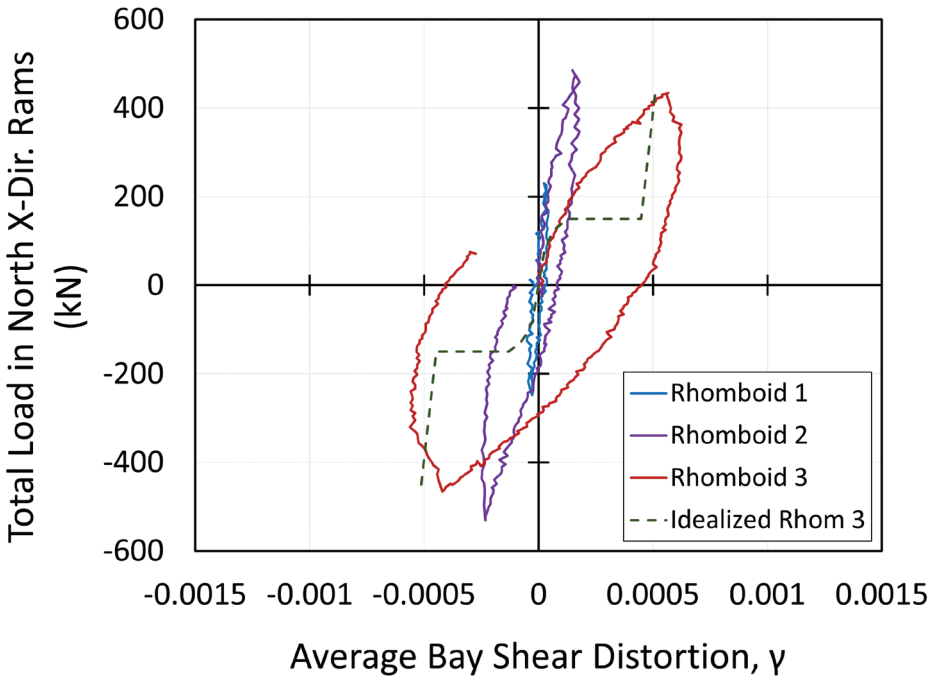

(a) Plan shear stiffness behaviour of the first three rhomboids of TEST 2 (for comparison with the TEST 1 rhomboids)

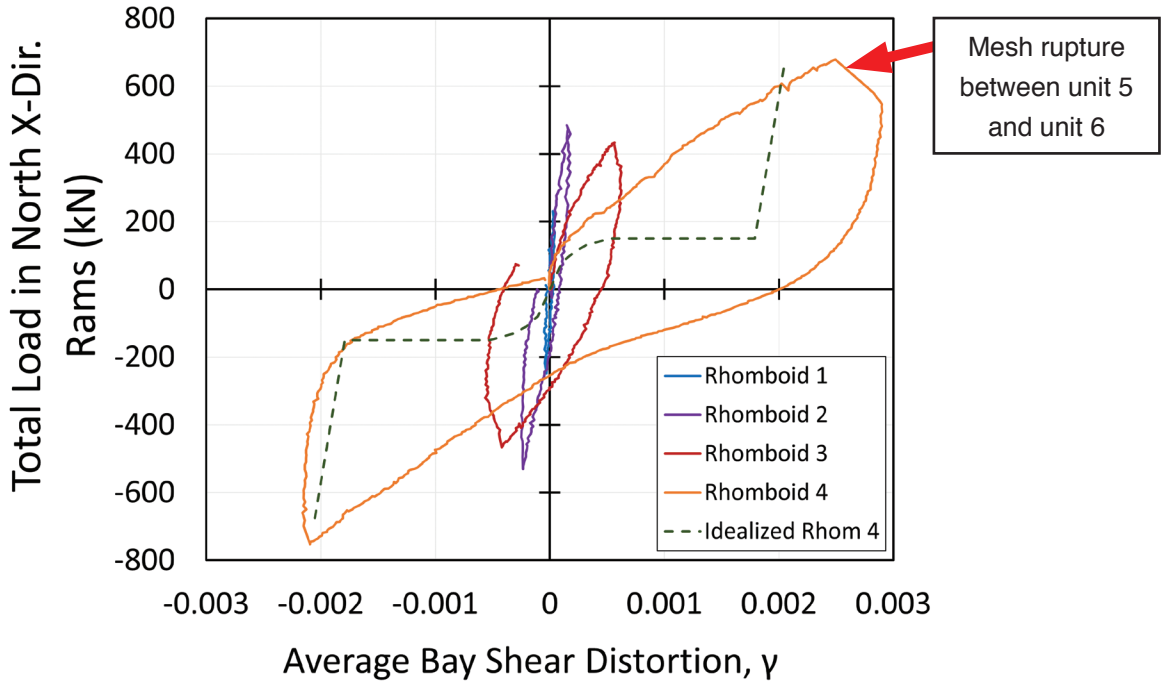

(b) Plan shear stiffness behaviour of all four rhomboids of TEST 2

Figure 9: Observed plan shear stiffness behaviour for the first three rhomboid loading protocols undertaken in TEST 2

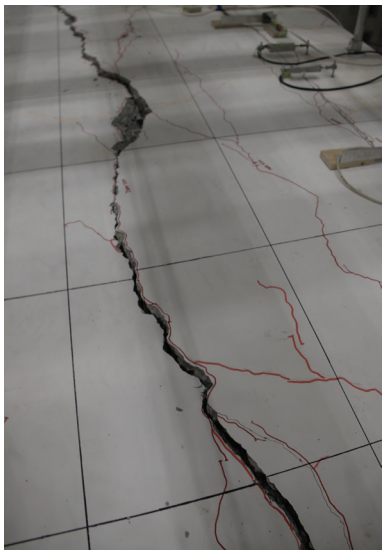

(a) Highly curved crack surface along A1B1

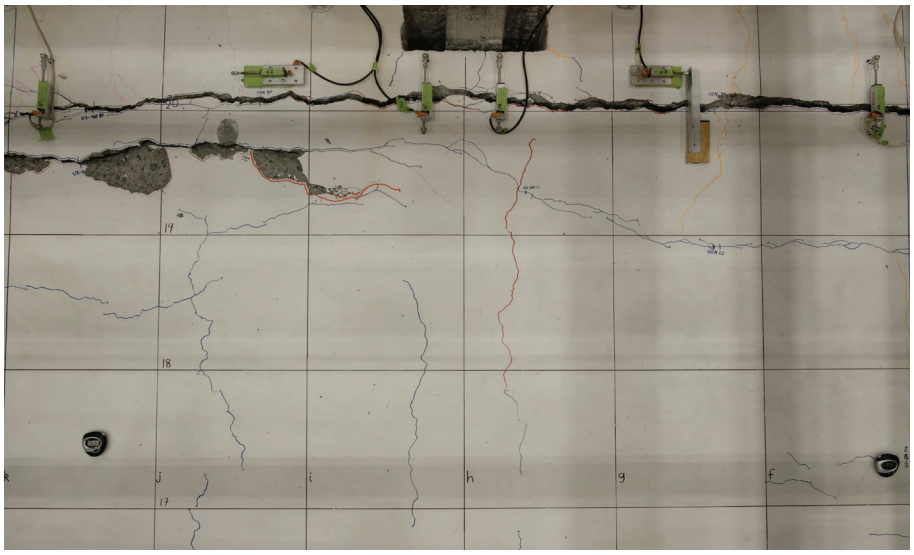

(b) Slightly curved crack surface along A2B2

Figure 10: Curved and rugged wide crack interfaces in TEST 2

There is a stark difference between the idealised and observed force-displacement results. Under real shear distortion loading there is an immediate resistance to shear deformation in plan at all damage states. The reason for the discrepancy becomes clearer when the crack patterns are considered. When considering the perimeter cracks theoretically, it was assumed that once a wide enough crack formed there would be no contact across the crack and it could be idealised as a gap similar to a saw cut, i.e., with a clean visible gap between the two sides. The reality of cracking in floors is that it does not result in clean, unobstructed cracks. Examples from the 2020 UC super-assembly experiments are displayed in Figure 10.

It is well known that aggregate interlock can transfer load at small crack widths (<0.3 mm) (Vecchio and Collins 1986). The process of aggregate interlock requires pieces of aggregate engaging with the other side of a crack. As cracks run through the weak points in the interfacial transition zones of the concrete, this creates a rugged, three-dimensional interlocking surface that can transfer compressive forces. The results from the super assembly tests showed that compressive forces can also transfer across crack widths much greater than 0.3 mm once aggregate interlock is lost. However, at this higher level of damage the process is different. For aggregate interlock, the two sides of the crack can remain mostly intact and close which contributes to compressive capacity under loading, as the gap is very small.

For the observed wide crack compressive load-path, it requires that rubble produced from grinding of the two crack sides falls into the existing gap and gets jammed at a tighter point in the crack. This means that the compressive load path at wider crack widths is a rubble aggregate contact stress compression mechanism. Reverse cyclic loading of a structure evidently provides enough grinding of the crack interfaces to create enough rubble to keep replenishing the compressive load path, up to surprisingly large crack widths. As new contact surfaces are created by jammed rubble, these new surfaces can also grind off protruding elements in the crack to generate more rubble. Also, cracks near the floor perimeter tend to be angled (such as the positive and negative moment-shear cracks that are causes for concern in hollow-core). This provides more locations for pieces of rubble to get stuck and jam than assumed clean vertical cracking would.

Cracks that form a curved surface are particularly effective at creating rubble to replenish the compressive load path. An example of this cracking layout from TEST 2 is displayed in Figure 10 (a). This cracking occurred along the ends of units near the interface with beam A1B1. It should be noted also that curved and angled cracking surfaces in the floor (relative to the primary axes of the structure) naturally developed near all corners and columns due to the simultaneous bi directionality of loading.

The most obvious case of load path replenishment from rubble was visible in TEST 2 where a large wedge of concrete at the topping near column B2 became

dislodged from both sides of the major crack and slotted into the gap, linking both sides of the crack. The concrete wedge is displayed in Part I (Parr et al. 2022). This wedge was unmoveable due to the compression it was under until 5% drift, which displayed how it was actively providing a compression load path up to this point. Over multiple cycles the wedge was pushed up by compression acting across inclined faces, so it was higher than the concrete on either side of it. Under reverse cyclic loading it would be expected that the wedge would rise and fall depending on the drift direction. Instead, it was continually pushed up. This displayed how additional grinding of the contact surfaces had created extra rubble, leading to the wedge being slowly squeezed out while remaining in compression.

The key conclusion to be drawn from these results is that diaphragm compressive load struts can be transferred across wide cracks. If there is a sustained gravity load path between the floor elements and the beam elements, a diaphragm compressive load path will also be sustained to much higher crack widths than previously anticipated. The limitation on crack width to sustain this contact stress compressive load path is unknown and would benefit from future research. A suggested assumption would be that the aggregate size used in the concrete mix is the maximum width before a reliable contact stress load path is lost, as individual pieces of aggregate are unlikely to crush. With distortion across cracks that have significant roughness and curved interfacial surfaces, cracks even wider than the aggregate size may be able to sustain intermittent struts. A depiction of compression strut formation across wide cracks due to aggregate rubble interlock is displayed in Figure 11. The aggregate size used in the TEST 1 and TEST 2 floor topping concrete mixes was 19 mm.

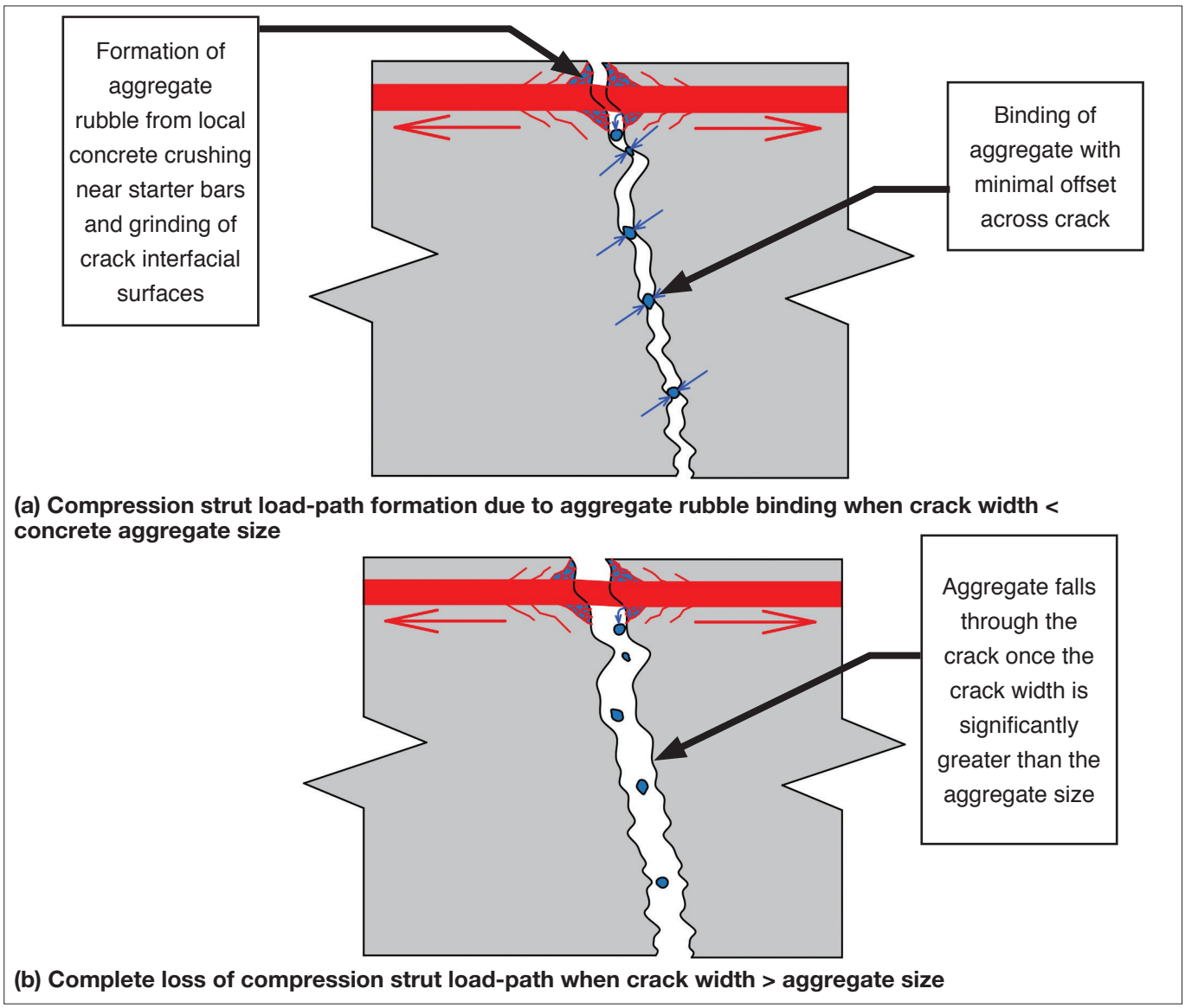

Figure 11: Residual compression strut load-paths forming across wide cracks due to aggregate rubble binding (Parr et al. 2022)

The finding that residual contact stress compressive load paths develop across wide cracks does not mean that strut-and-tie load paths remain unaffected through all damage states. If mesh rupture occurs as it did at the end of the starter bars along beam A1B1, tension tie load-paths are eliminated. Additionally, as discussed in Part I (Parr et al. 2022), gaps had opened around all the interfaces between columns and floor elements by 1% to 1.5% drift in both tests. As these interfaces were vertical and smooth, the rubble load path replenishment seen in the floors did not apply to these gaps. This meant that it would not have been appropriate to make the assumption for struts landing directly onto columns typical in strut-and-tie analysis in the case of a relatively small earthquake (the exception to this generally observed rule occurred only for the interior column to floor interfaces that were connected by tie bars as discussed later in Part I (Parr et al. 2022) and Section 2.3 of Part II).

Therefore the only remaining load-path for diaphragm compression struts to land into the rest of the structure was through the beams. While this held true for both TEST 1 and TEST 2, the exact form of the load-path degradation and rate of stiffness degradation was different. This was caused by the difference in load-path directionality between experiments and the stitching retrofit employed to keep the beta units together in TEST 2 which was not used in the TEST 1. Improved roughening of beam-column cold joint casting interfaces in TEST 2 described in Part I (Parr et al. 2022) likely also caused differences in the point diaphragm degradation initiated.

The secant stiffnesses obtained from both the TEST 1 (1:1 standard loading directionality ratio) and TEST 2 (1:2 standard loading directionality ratio) rhomboid loading sequences relative to the previous maximum drift the structure had been pushed to are displayed in Figure 12. The measured applied force divided by the shear strain, F_{rhom}/γ, is displayed in Figure 12 instead of the effective shear modulus, G_{eff}. This is because the effective shear surface area between the frame and floor elements, A_{eff}, is likely a changing variable as damage increases and requires further research. Thus a reliable value for G_{eff} cannot currently be obtained to provide a typical shear stress/strain relationship. Also note the effective shear modulus, G_{eff}, is not an elastic shear modulus (G) as elements of the system had experienced plastic deformation and cracking for all datapoints. The relationship between G_{eff} and F_{rhom}/γ is shown in Equation (1):

$$G_{eff} = \frac{\tau}{A_{eff}} = \frac{F_{rhom}}{A\gamma} \quad (1)$$

Rearranging provides the relationship in Equation (2):

$$\frac{F_{rhom}}{\gamma} = G_{eff} A_{eff} \quad (2)$$

The green dot and line in Figure 12 (a) depict the first rhomboid of TEST 2. At this stage in testing only uni-directional drift demands of 2% in the -Y drift direction

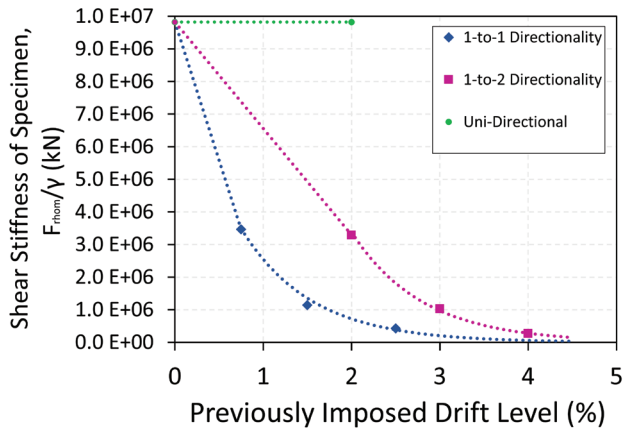

(a) Absolute values of plan shear stiffness

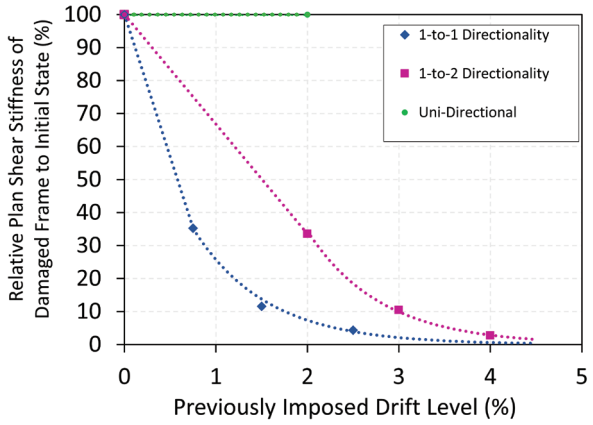

(b) Relative values of shear stiffness ($\%G_{initial}$) compared to the initial observed stiffness in TEST 2 rhomboid #1

Figure 12: Residual compression strut load-paths forming across wide cracks due to aggregate rubble binding (Parr et al. 2022)

and 1% in the +Y, -X and +X directions had been applied to the specimen. As discussed in Part I (Parr et al. 2022), cracking had developed in the floor at this stage but there had been no signs of mesh rupture or loss of beam torsional stiffness. This is therefore the closest experimental data-point to an idealised design value that may be obtained from a strut-and-tie or grillage method. Future research should seek to compare this experimentally obtained diaphragm shear stiffness value to these commonly used modelling methods.

Figure 12 shows that the rate of plan shear stiffness degradation is heavily dependent on the directionality of the earthquake. As discussed in Part I (Parr et al. 2022), TEST 1 was designed to replicate an upper bound for earthquake directionality while the TEST 2 experiment was designed as a lower bound for realistic directionality of earthquakes. Therefore by interpolating between the 1:1 directionality and 1:2 directionality lines in Figure 12, a full range of diaphragm stiffness degradation rates relative to the earthquake directionality ratio can be obtained. The equations for the 1:1 directionality stiffness degradation relationship are provided in Equation (3) and (4), where $\%G_{\text{initial}}$ is the diaphragm shear stiffness percentage relative to the initial stiffness and θ is the maximum drift demand (% drift) experienced by the structure.

$$\%G_{\text{initial}} \approx 100 - 86\theta, 0 \le \theta \le 0.75 \quad (3)$$

$$\%G_{\text{initial}} \approx 90e^{-1.25\theta}, 0.75 < \theta \le 2.5 \quad (4)$$

The equations for the 1:2 directionality stiffness degradation relationship are provided in Equations (5) and (6), where θ is the maximum drift demand (% drift) experienced by the structure.

$$\%G_{\text{initial}} \approx 100 - 33\theta, \ 0 \le \theta \le 2 \quad (5)$$

$$\%G_{\text{initial}} \approx 416e^{-1.25\theta}, \quad 2 < \theta \le 4 \quad (6)$$

Based on these equations, a generalised set of equations for earthquake directionality is provided in Equation (7) and (8), where θ is the maximum drift demand (% drift) experienced by the structure and α is the ratio of drift demand between the drift in the primary loading direction and drift in the minimal loading direction (typically orthogonal to the primary loading direction).

Note that generalised Equation (8) is fitted to provide close alignment with Equation (7) at 1:2 (50%), 3:4 (75%) and 1:1 (100%) directionality ratios (α). There is a slight discontinuity between the two equations at other directionality ratios. This discontinuity can be removed by altering the 0.76 factor at the start of Equation (8).

Also shown in Figure 12 is the stiffness of the specimen following uni-directional pushes up to 2% in the Y-direction and 1% in the X-direction (following the initial Northridge earthquake portion of TEST 2). As seen in Figure 12 (a), this is much stiffer than the specimen when it was subjected to lower drift levels of simultaneous bi-directional loading. Due to the high stiffness and low damage at this stage in TEST 2, the value obtained from this rhomboid loading of 9.82 x 10^6kN per radian distortion was taken as the benchmark 100% plan shear stiffness to compare against in other rhomboid loading protocols. Due to the nature of the standard loading protocol used in the two tests, there was no further data obtained for the degradation of the diaphragm under uni-directional pushes. However, other research has investigated the plane shear stiffness of pre-cast floor diaphragms without pre-damaging the floor (Angel et al. 2019). The stiffness behaviour of diaphragms that are undamaged or have been subjected only to uni-directional drift demands would match the data obtained from these experiments more closely.

A limitation of the rhomboid data is the approximately 0.1 mm ±0.05 mm accuracy of the draw-wires used in measuring deformations. Particularly for rhomboid #1 of TEST 2, which saw maximum displacements of 0.4 mm, this translates to a ±12.5% error which is directly carried into the estimate of the diaphragm stiffness at its least damaged state. As the purpose of the experiment was to capture the general trends of the stiffness degradation without impacting the reliability of subsequent rhomboid loading protocols, this error is viewed as acceptable.

Additionally, as there is no data from rhomboid loading protocols conducted between 0%-0.75% drift for TEST 1 and 0%-2% drift for TEST 2, a linear interpolation has been used in this range (described in Equations 3, 5 and 7). This interpolation was from 100% stiffness for the undamaged specimen, directly to the first rhomboid stiffness result following simultaneous bi-directional demands.

It is likely that this interpolated estimate overestimates stiffness degradation at low drifts within the frame elastic response range (e.g. 0-0.25%). Future research could attempt to provide more representative results for low drift demands using methods to estimate elastic stiffness of the diaphragm .

$$\%G_{\text{initial}} \approx 100 - \frac{6.5 - 3.5(\alpha - 1)}{0.75 - 2.5(\alpha - 1)}\theta, \ 0 \le \theta \le 0.75 - 2.5\ (a - 1) \quad (7)$$

$$\%G_{\text{initial}} \approx (0.76 + 0.96|\alpha - 0.75|)*(90 - 650\ (\alpha - 1))*e^{1.25\theta}, 0.75 - 2.5(\alpha - 1) < \theta \le 4 \quad (8)$$

Finally, the exponential portion of the obtained Equations (Equations 4, 6 and 8) only have backing data up to 2.5% drift for 1-to-1 directionality and 4% drift for 1-to-2 directionality. Reliability of results is lower beyond these drift levels. However, with these drift levels the remaining diaphragm shear plan stiffness is less than 5% of the initial stiffness, so this is a minor consideration.

In TEST 1 and TEST 2, the plan shear stiffness was observed rapidly decreasing from the original diaphragm stiffness under simultaneous bi-directional loading. As the degree of simultaneous bi directionality was within realistic levels, this means the rigid diaphragm assumption may not be appropriate when modelling building response. An interesting aspect to this result is that diaphragm shear stiffness degradation was clearly not primarily driven by wide cracks in the floor as initially expected, as the largest stiffness losses occurred prior to wide cracks opening.

2.2 PRIMARY DIAPHRAGM STIFFNESS SOFTENING MECHANISM

The reason for stiffness degradation of the diaphragm was not due to the expected loss of load-path across wide cracks in the floor, but instead due to degradation of the only remaining portion of the load-path into the columns; the beam plastic hinges. After a compressive strut lands on a beam, the load must then be transferred through the plastic hinge in shear about the weak axis of the beam as displayed in Figure 13.

The beam plastic hinge degradation was driven in the form of loss of torsional stiffness. Loss of beam torsional stiffness after a frame has been subjected to earthquake loading has been observed in previous tests with frames specimens incorporating floor diaphragms, but it has not previously been identified as for a major contributor to diaphragm plan shear stiffness degradation. A depiction of a beam that has lost torsional stiffness in the plastic hinge zone is displayed in Figure 14.

Based on the TEST 1 and TEST 2 observations the process of a beam losing torsional stiffness appears to require the following events to occur:

- Beam elongation must proceed to a stage where aggregate interlock across the primary crack near the beam-column interface is reduced as shown in Figure 15.
- Weak-axis and torsional demand applied from the floor elements connected to the beam must reach a level where it overpowers the combined capacity of the beam longitudinal bars acting in dowel action across the primary crack and friction between the interfaces of the two sides of the crack acting in compression through contact stresses as shown in Figure 16. Note that there are four combinations of simultaneous bending between the two orthogonal beam directions. Based on the direction of twist and location of damage in the beams observed at the end of both tests, the critical load combination was identified as negative bending in the beam of interest (tension at the top critical beam longitudinal bars) and negative bending in the orthogonal beam (tension in the top orthogonal

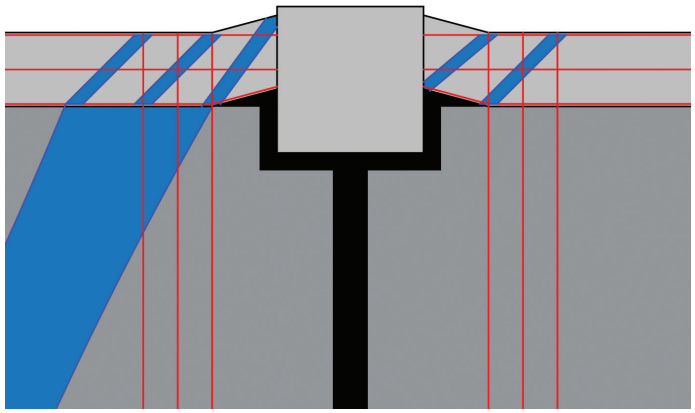

(a) Into an intermediate column

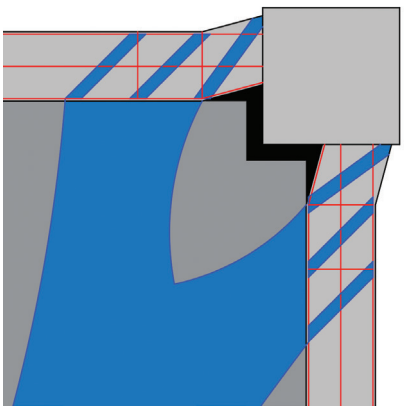

(b) Into a corner column

Figure 13: Transfer of diaphragm compressive struts through beam plastic hinges (compressive struts depicted in blue and tension ties in red)

beam longitudinal bars and starter bars). Based on which longitudinal bars were most heavily loaded in tension, the centre of torsional stiffness in the beam moved, meaning the instantaneous centre of rotation (ICR) also moved. By the end of the test, the buckling of the interior bottom beam bars depicted in yellow in Figure 16 (d) and (e) had permanently moved the ICR to the bottom outer corner of the beam, as evidenced by the torsional distortion observed.

The proposed reason that loss of beam torsional stiffness degrades the diaphragm plan shear stiffness is, as the beam twists, it buckles the interior bottom bars, thus cracking the surrounding concrete and reducing their confinement and bond with the rest of the beam. This decreases their contribution to dowel action by not having an effective, supported length determined by the stirrup spacing, which is a much weaker and less stiff contribution to the beam shear load path than the originally designed confined shear contribution. Additionally, twisting of the beam across the primary crack near the beam-column interface likely grinds the two sides of the crack smoother over multiple cycles, reducing aggregate interlock and the friction necessary to

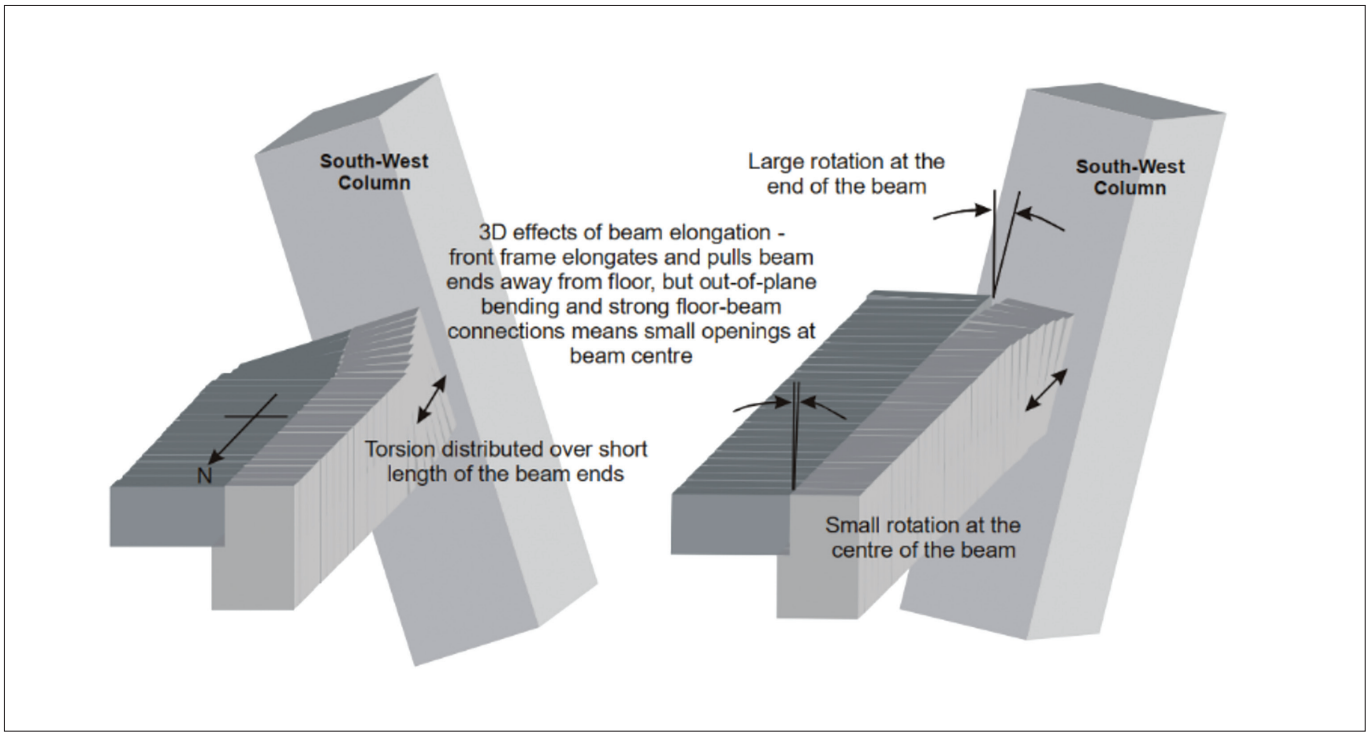

Figure 14. Beam torsion observed in previous UC super-assembly experiments (MacPherson, 2005)

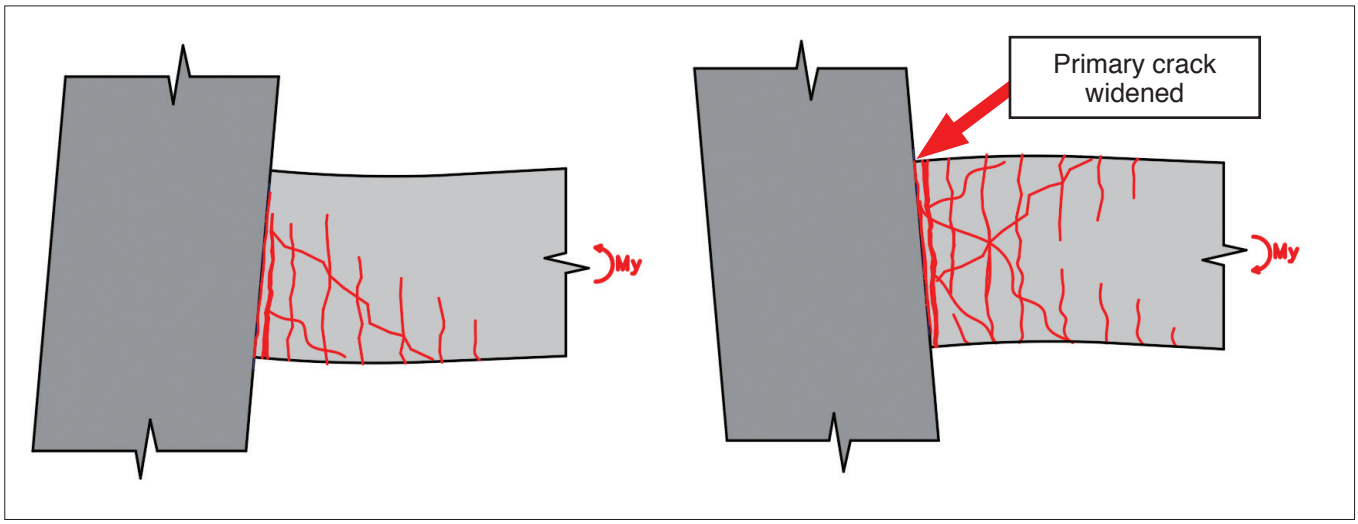

Figure 15: Primary wide crack/s forming near the beam-column interface developing due to beam elongation

maintain the compressive portion of the weak axis shear load-path. This damage would reduce the minor axis shear capacity of the beam, reducing the strength of the load-paths depicted in Figure 13.

While this appears to be a relatively simple process, there are a wide range of factors that can change the level of drift required to initiate loss of beam torsional stiffness as well as changing the level of its impact and rate of degradation once initiation occurs. These factors are a set of interconnected phenomena that can alter the order of occurrence of damage modes for the overall floor system.

The most critical interconnected factors are:

- Degree of simultaneous bidirectionality in earthquake loading.
- Amount of beam elongation.
- The ratio of beam plastic hinge cross-section strength to imposed demands from the floor-beam connection on half the beam span.

For more in-depth investigation into the inter-relationship of these and other factors on the rate of diaphragm shear stiffness degradation refer to (Parr 2022).

Figure 16: Process Leading to Loss of Beam Torsional Stiffness

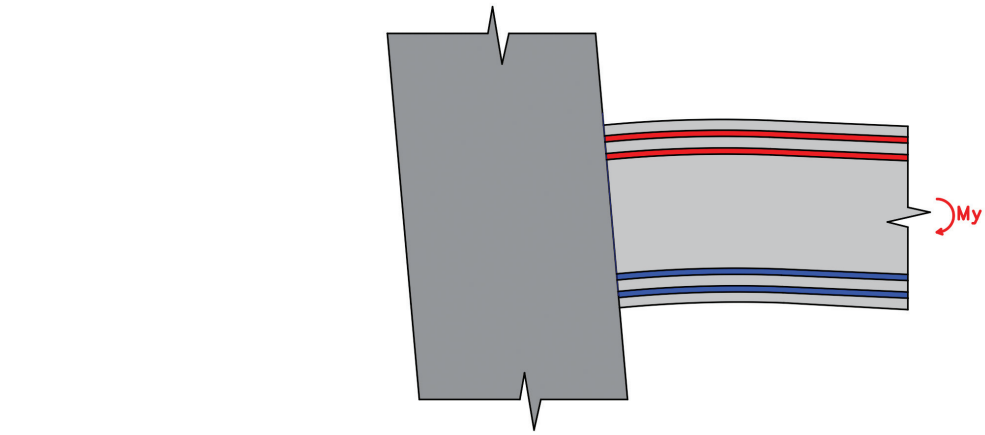

(a) Side view of the critical beam under negative drift demands (top beam bars in tension)

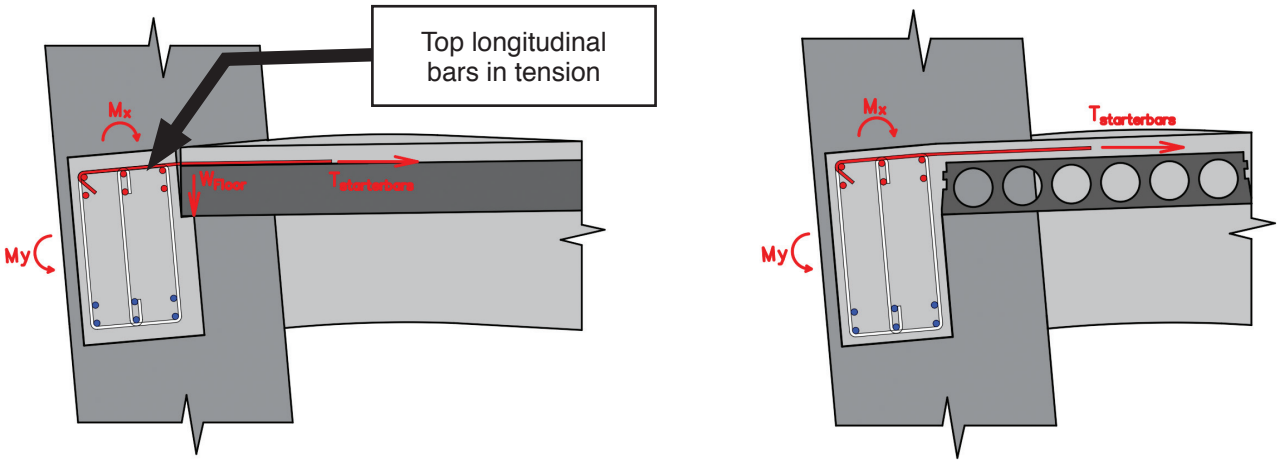

(i) Support beam variant demands **(ii) Longitudinal beam variant demands**

(b) Cross-section view of the critical beam with demands from orthogonal beam in negative bending (top beam bars and starter bars in tension)

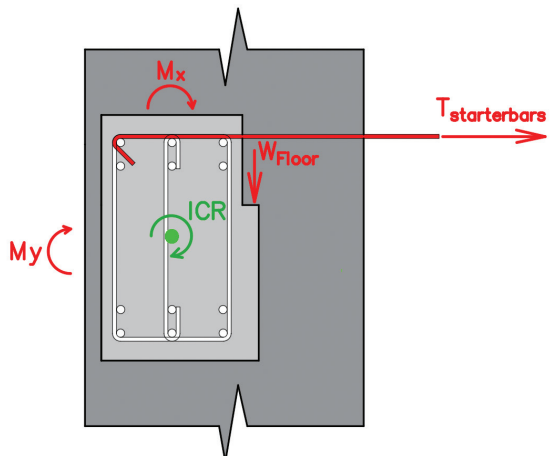

(c) Initial ICR with Critical Beam Load Combination Shown

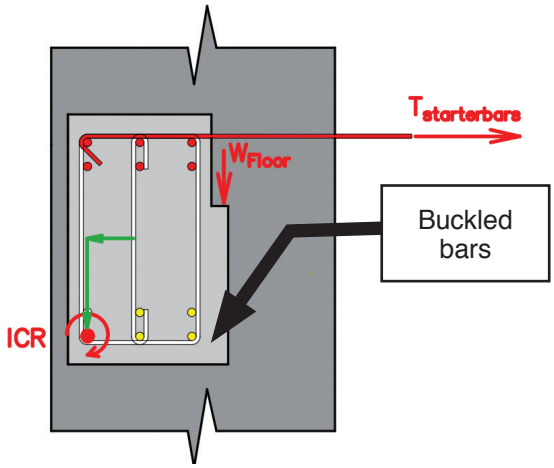

(d) Movement of ICR as Yellow Highlighted Bars Buckle Under Torsional Demands

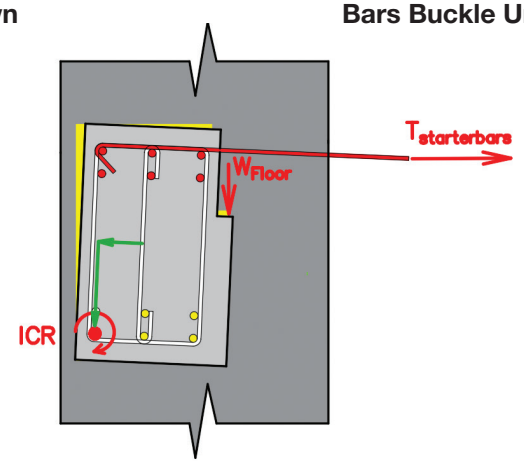

(e) Torsional Rotation of Beam Through the Plastic Hinge About the Residual ICR

2.3 EFFECTS OF THE SIMULTANEOUS BI-DIRECTIONALITY RATIO AND TENSION TIE RETROFITS ON DAMAGE MODES AND DIAPHRAGM STIFFNESS DEGRADATION

2.3.1 Test 1

As discussed in Section 2.1 TEST 1 yielded unexpected and interesting results based on the chosen directionality of the standard loading protocol. The 1:1 directionality (circular rather than elliptical) was selected primarily to provide a worst-case scenario for the individual hollow-core units by enforcing maximum realistic simultaneous strong-axis, weak axis and torsional demands along the lengths of the units via deformation incompatibility with the ductile support beams. Instead it was observed relatively early (by approximately 1.5% drift) that the beams became overloaded by the simultaneous actions caused by deformation incompatibility with the diaphragm and lost torsional stiffness. The loss of beam torsional stiffness meant the support frame for the diaphragm was no longer stiff enough to impart large enough forces through the floor starter bars to damage the floor units. In effect, the weak link in the capacity hierarchy for the system was the beams rather than the floor itself. Diagrams of the demands applied to support and longitudinal beams while experiencing simultaneous bi-directional loading are displayed in Figure 16.

Based on the loss of load-path through the beta-beta unit interface and the inability for diaphragm compression struts to land directly into columns the remaining shear deformation strut load-path in TEST 1 from 1.5% drift onward is displayed in Figure 17.

This load-path is similar to the “picture frame effect” proposed in section 1, except it requires landing of struts in the beams instead of directly between columns. Note that the compression struts displayed in Figure 17 are a simplification for clarity of the true paths a diagonal strut within the floorplate could take. As seen in the crack

patterns in Figure 4, intra-span and beta units of each bay acted as a single block. This means tension ties within and across these units were viable to allow for a truss-like strut-and tie system within each bay. Struts tend to form at an angle of less than approximately 60° (referencing the axis of the support beams), meaning it is probable that tie-backs developed in the system to provide a lower energy load-path like the one displayed in Figure 18. This applies to all subsequent diaphragm load-path figures.

The observation of concrete crushing in the plastic hinge of beam B2C2 near column C2 under positive shear distortion demands and in the plastic hinge of beam B1C1 near column C1 under negative shear distortion demands provided evidence of significant tension ties forming in the north-south direction across the floorplate as shown in Figure 17 (b). These tension ties engaged the beam plastic hinges of the support beams that were not on the short diagonals of the distorted floorplate. The ties also enforced the bowstring effect on each individual bay with elongation of the longitudinal beams restricted (in theory) by the tension ties linking the support beams.

The initial undamaged stiff diaphragm had tension ties running across the entire floorplate in both the north-south direction linking the support beams and in the east-west direction linking the longitudinal beams. This meant that in both directions the bowstring effect was restricting beam elongation (so elongation of both the support and longitudinal beams were being restrained by tension across the floor). After splitting and mesh rupture occurred between the beta units at the start of the 1.5% drift cycle, the bowstring effect in the east-west direction was eliminated. This meant beam elongation of

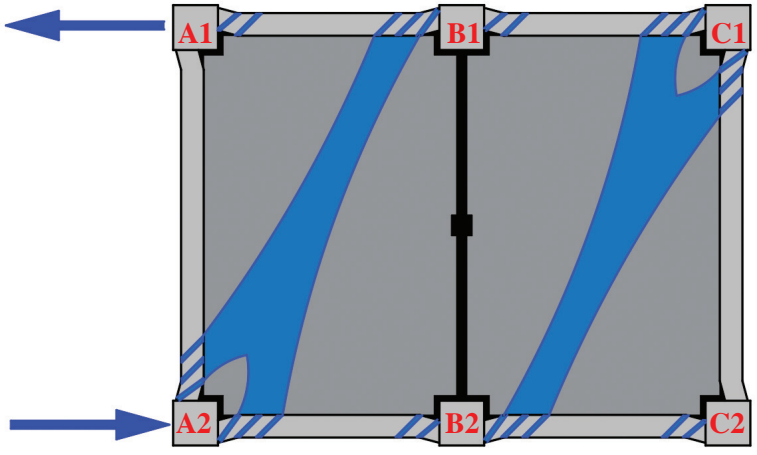

(a) Load-path with only compression struts

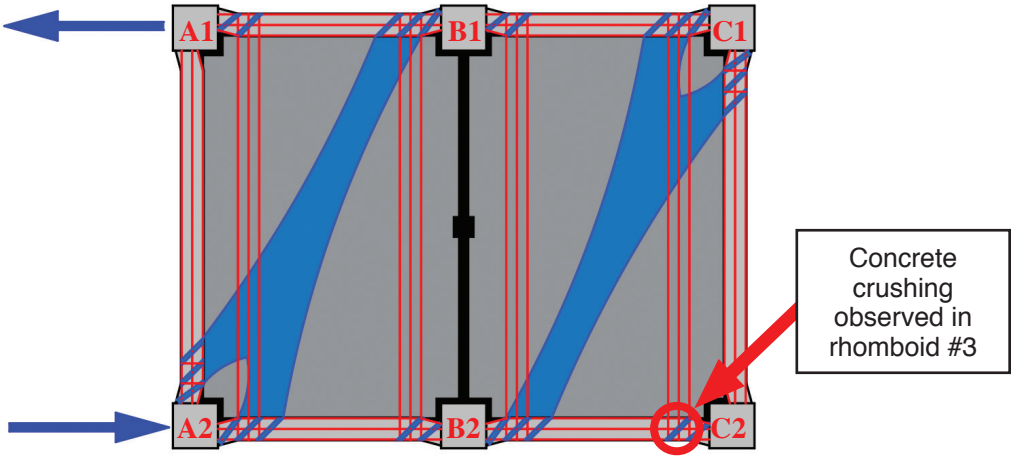

(b) Load-path with struts and tension ties

Figure 17: TEST 1 Residual diagonal compression strut load-path under positive shear distortion loading

the support beams was no longer restrained. As shown in Figure 19, beam elongation of beams A1B1 and B1C1 rapidly increased from this point on.

An unexpected outcome from this data is the finding that the longitudinal beam elongated as much as the support beams beyond 1.5% drift. With tension ties linking the support beams and the bowstring effect intact in this direction, it could be expected that elongation would be lower in the longitudinal beams from restraint through the floor. The reason this was not the case is evident if the torsional response of each beam is examined. This is displayed in Figure 20.

Figure 20 (a) and (b) show that beyond the loss of the east-west bowstring effect the support beams rotated into the span, meaning the distance between the starter bar connections of the north and south support beams was reduced. This meant the bowstring effect restricting longitudinal beam elongation was greatly reduced, because the bowstring ties were anchored in weak, flexible beams. The direct correlation between the longitudinal beam elongation and support beam rotation is clearer in Figure 21. Once the east-west bowstring effect is lost and the support beams lose torsional stiffness, each elongation of the longitudinal beam A1A2 is directly followed by inward rotation of the support beams to accommodate the growth in the orthogonal direction. This displays that once the bowstring effect is lost in one direction, the run-on effects of beam elongation and torsion of the affected beams leads to loss of effective bowstring action effects in the orthogonal direction. It also displays that while the bowstring effect restrains and stiffens the diaphragm system at low levels of damage, it is a direct driver of diaphragm plan shear stiffness degradation at higher damage levels by enforcing large torsional demands on the beams, leading to beam loss of torsional stiffness and therefore reduction of beam weak-axis shear stiffness in the plastic hinges.

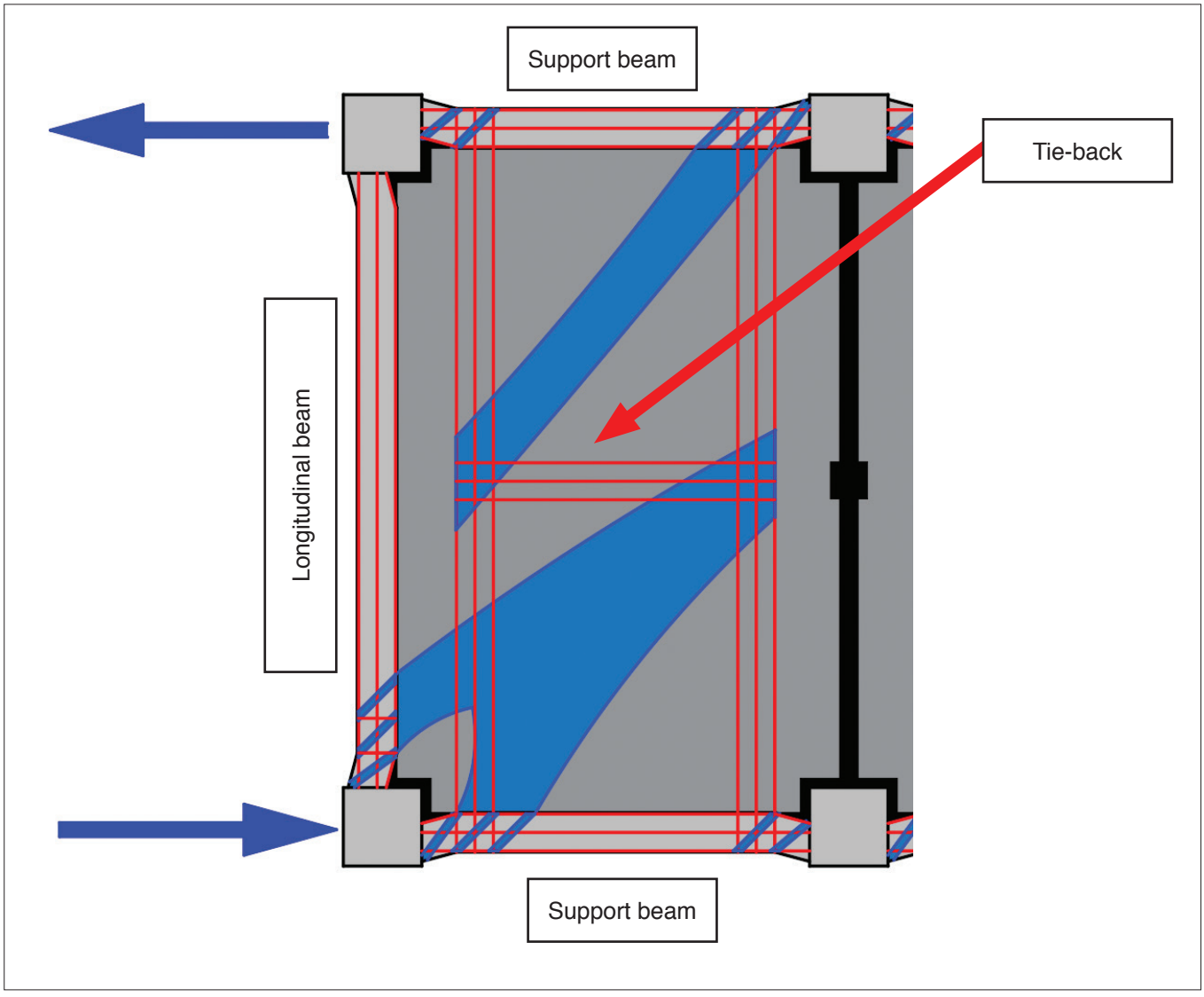

Figure 18: Diagonal struts with tie-backs to form low energy truss strut-and-tie load paths within the floor-plate

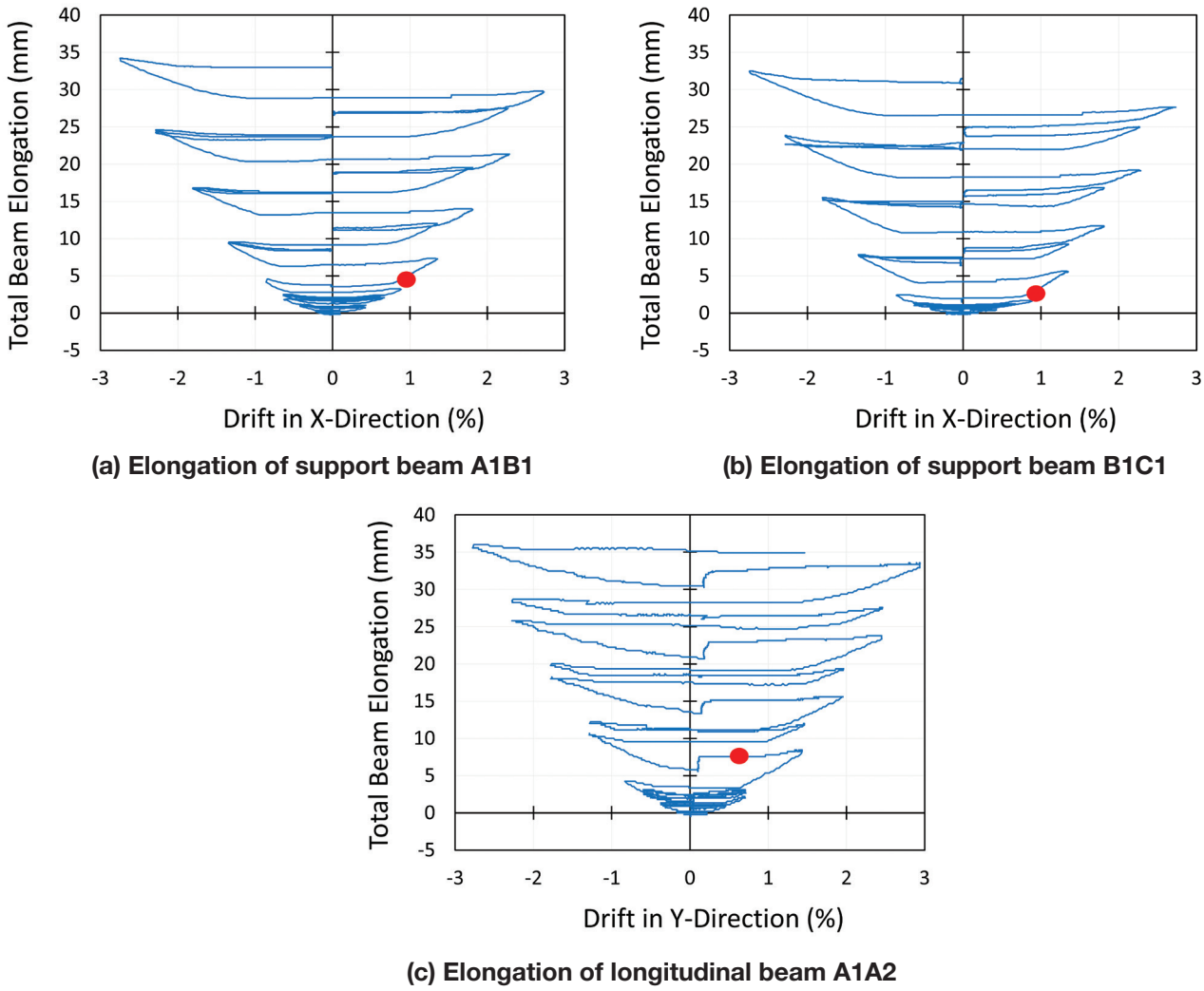

Figure 19: TEST 1 Elongation of support and longitudinal beams relative to their critical loading direction (red dots indicate where the bowstring effect was lost for support beams)

Inward rotation in Figure 21 describes the top of the beams (where they are connected to the floor via starter bars) moving inwardly towards the floorplate. A visual representation of this and the starter bar demands that cause it is portrayed in Figure 16 (e).

The torsional rotation of beam A1B1 and B1C1 is nearly identical. As discussed in Part I (Parr et al. 2022), the first (eastern) bay had only starter bars crossing the beam-floor interface whereas the second (western) bay had both mesh and starter bars crossing the interface, increasing the interface capacity and therefore the total torsional demands that could be imparted into the beam via the bowstring effect. The lack of any noticeable difference between the behaviour of the two beams suggests that the starter bar-only configuration was already overpowering the torsional capacity of the support beam and further reinforcement across the beam-floor interface had no effect on the diaphragm capacity. This suggests the standard starter bar detailing provided over-reinforcement and the amount of beam-floor continuity reinforcement could have been reduced with no negative repercussions for the diaphragm performance.

The diaphragm load-path displayed in Figure 17 assumes there is no ability to transfer compressive load struts directly into columns. This is a valid representation of the available load-paths observed at earlier stages of the test after gaps had opened around the columns, as there were clear air gaps preventing any load-path from forming

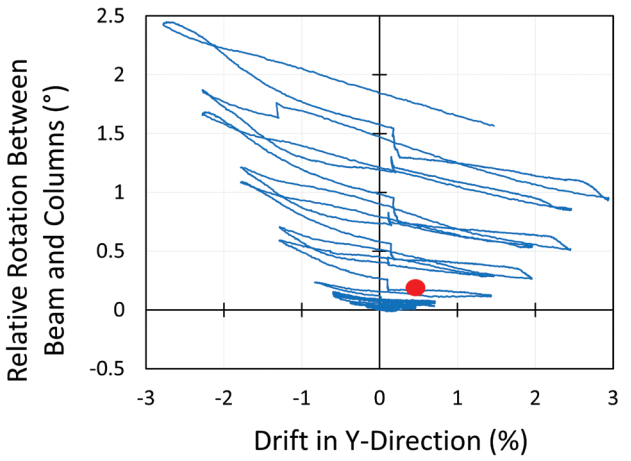

(a) Torsional rotation of support beam A1B1 relative to columns A1 and B1

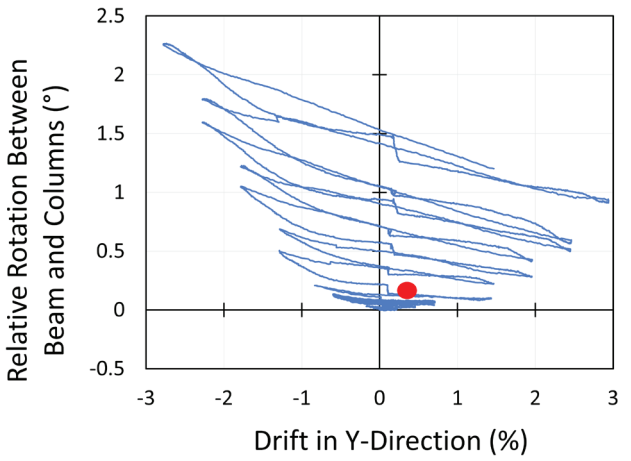

(b) Torsional rotation of support beam B1C1 relative to columns B1 and C1

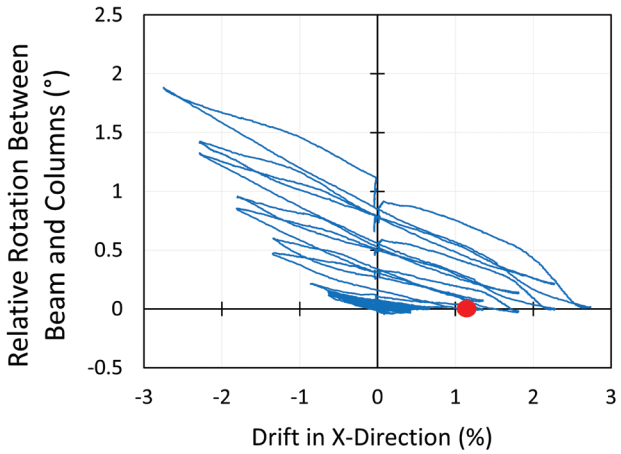

(c) Torsional rotation of longitudinal beam A1A2 relative to columns A1 and A2

Figure 20: TEST 1 Torsional rotation of support and longitudinal beams relative to their supporting columns (red dots indicate where the bowstring effect was lost for support beams)

for all columns. This applied to the intermediate columns as only the tie bars linked the two sides of the gap, which would provide a minimal strength compression/shear load-path when compared to the scale of the overall diaphragm forces.

However, in the final rhomboid loading of TEST 2 there was clear evidence of compression struts forming directly between the floor system and the intermediate (B1 and B2) columns as shown in Part I (Parr et al. 2022). The TEST 1 residual load-path with the addition of this tie-bar rubble contact stress compression load-path is displayed in Figure 22.

As the specimen was pushed to greater drifts and the diaphragm subjected to greater deformation in both tests, chunks of the floor topping slab around each tie-bar connection were popped off in a flat cone pull-out style failure mechanism as displayed in Part I (Parr et al. 2022). Pieces of the rubble formed in this way appeared to drop into the gap between the floor units and the column, instating a residual contact stress load-path (from approximately 2%-2.5% drift onwards) for compression struts, similar to the ones that had formed along the beams in TEST 2. Without the tie-bars and the rubble formation they caused, no load-path could form from

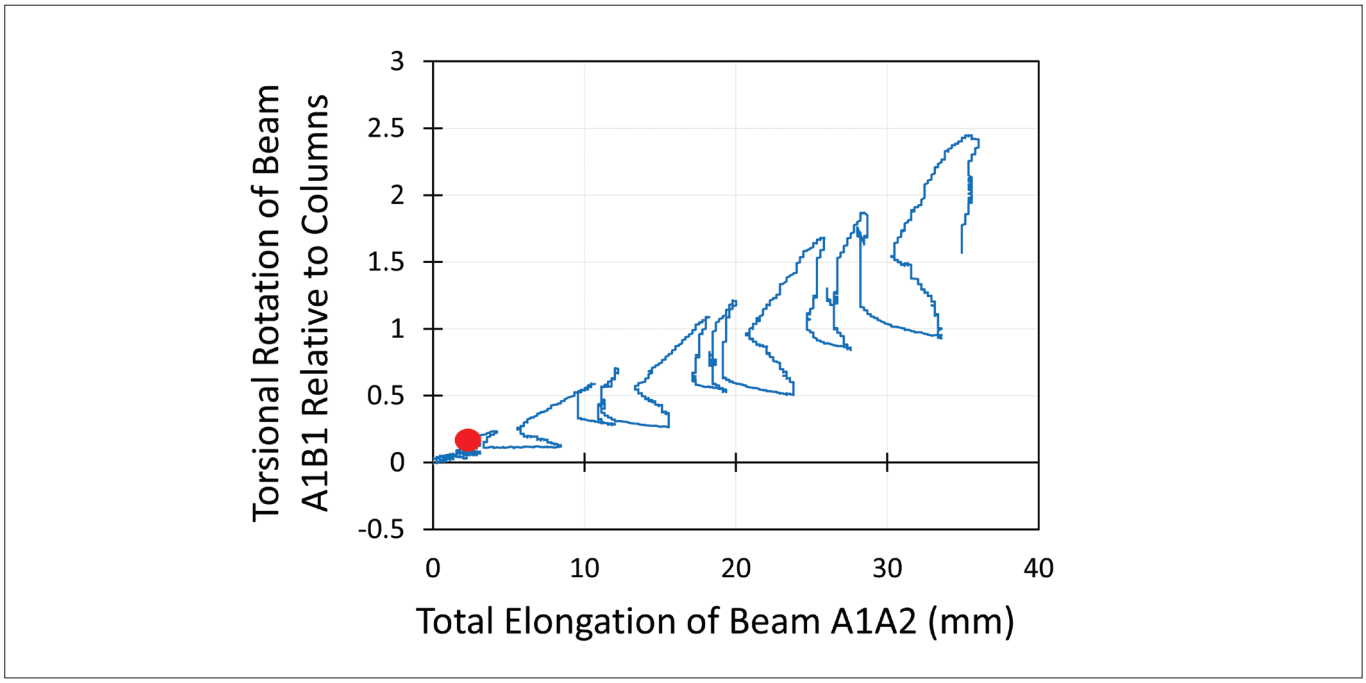

Figure 21: TEST 1 Inward rotation of support beam A1B1 driven by elongation of the orthogonal longitudinal beam A1A2

the floor directly into the interior columns. This displays a secondary positive effect caused by installation of tie-bars additional to the original intended purpose of restraining columns from pushing out of the building.

Important notes related to the tie-bar rubble residual contact stress compression strut load-path are:

- It could only form on the column face the tie-bars were anchored into.
- It required reverse cyclic behaviour to form rubble from compatibility demands between the tie-bars and floor topping.
- There may be a zone at moderate drift/damage levels where there is no load-path between the floor and column interface after the column-to-floor gap has opened but before sufficient rubble has been generated to instate the residual load-path.
- It was a stiffer load-path than struts landing in the beams, meaning higher potential for local concrete crushing damage to beta units which are already vulnerable elements of the floor system.
- It incorporated the tie-bars into the diaphragm system as tension ties.
- It incorporated the longitudinal beams into the diaphragm as anchor points for tension ties.

2.3.2 Test 2

TEST 1 displayed two critical results informing the design of TEST 2.

The first was that a high ratio of simultaneous bi-directional demands led to beams being the weak element of the system due to loss of torsional stiffness. Based on this finding, the loading protocol of TEST 2 was changed to an initial uni-directional push (based on the Northridge earthquake of 1994) followed by a lower-bound standard loading protocol simultaneous bi-directionality ratio of 1:2. This change was selected in an attempt to observe different damage modes in the hollow-core units and diaphragm by enforcing less critical demands for the beam torsional response and therefore more critical demands for the floor elements.

The second was the split in the weak zone between beta units leading to separation of the two bays of the floorplate. The removal of any diaphragm load-path linking the two bays and the destruction of the bowstring effect in the east-west direction at 1.5% drift was a defining point for the performance of the diaphragm from this point on for TEST 1. In TEST 2, “stitching bars” were post-installed in the topping between the beta units to replace the topping mesh reinforcement across the interface that was cut due to post-installation of tie-bars between column B1 and B2. This also provided the opportunity to compare the performance of the

diaphragm if the two bays remained linked and the east-west bowstring effect remained intact.

As discussed in Part I (Parr et al. 2022), much greater damage through the development of wide cracks was observed in the floor elements in TEST 2 compared to TEST 1, particularly at the seating ends of the hollow-core units. This damage mode initiated within the uni-directional push at the start of the test and further damage concentrated at the critical cracks. Mesh rupture across the north and south critical cracks occurred at approximately 1.6% drift (in the y direction). This signalled that the simultaneous bi-directionality ratio was critical in determining the damage mode of the floor, particularly at the start of loading. In floor systems that only use non-ductile mesh for topping reinforcement within the floorplate, damage will concentrate where it first occurs as the mesh will rupture at relatively low drift levels and further damage will concentrate at the weak zone this creates.

However it was also observed that compression struts could form across wide cracks via contact stresses with pieces of rubble that fell into the cracks. The residual load-path created by the damage modes observed in TEST 2 are displayed in Figure 23. The critical wide cracks near the ends of the units are displayed in green.

Note that while compression struts could cross the wide cracks at the ends of the hollow-core units, the cracks eliminated tension ties that crossed them in the north-south direction due to mesh rupture. This meant the bow-string effect in the north-south direction was eliminated

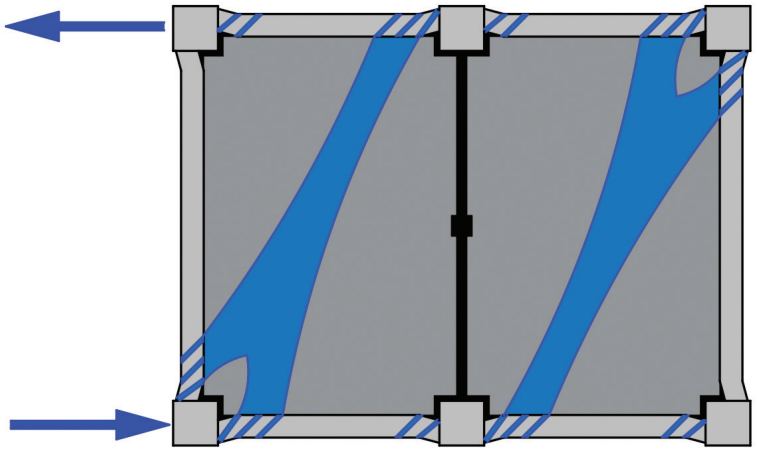

(a) Load-path with only compression struts displayed

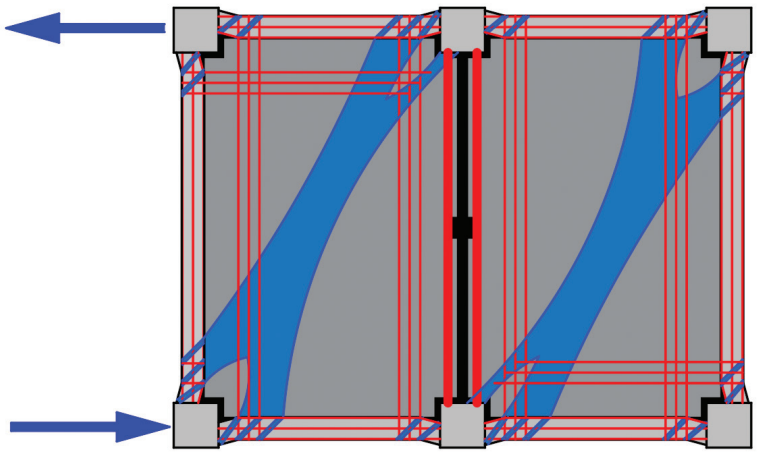

(b) Load-path with struts and tension ties displayed

Figure 22: TEST 1 Residual diagonal compression strut load-path under positive shear distortion loading after formation of tie-bar rubble contact stress compression struts

before the end of the uni directional pushes and before the standard loading protocol with a simultaneous bi-directionality ratio of 1:2 had begun.

The stitching bars were highly effective at strengthening the weak interface between the two beta units, and no significant cracking developed between the units even when drift demands of 4.0% in the N-S direction and 2.0% in the E-W direction were applied. This meant the bow-string effect in the east-west direction remained intact up to this point as shown with the ties linking the longitudinal beams in Figure 23. Without the strengthening across the weak beta-beta unit interface, this tension tie load-path would likely have been eliminated by 1.5% drift in the X-direction, greatly reducing the diaphragm plan shear strength (and therefore stiffness as a run-on effect), similar to TEST 1. Additionally, diagonal compression struts could form across both bays of the specimen with the two bays acting as a single diaphragm instead of two individual split diaphragms.

Following the 4% N-S, 2% E-W drift cycle, the 4th rhomboid of TEST 2 was conducted. At this stage in testing the cracks at the northern ends of the floor units were extremely wide, with approximately 30 - 40 mm crack widths (along the A2B2 and B2C2 beam-to-floor interface). At this crack width, even with replenishment of the compressive load-path through rubble formation, the gap was clearly wide enough to prevent effective compressive struts from forming. This led to loss of load-path across the crack as depicted in Figure 11 (b). The crack width at the southern end of the floor units at the end of the starter bars was approximately 20 mm wide

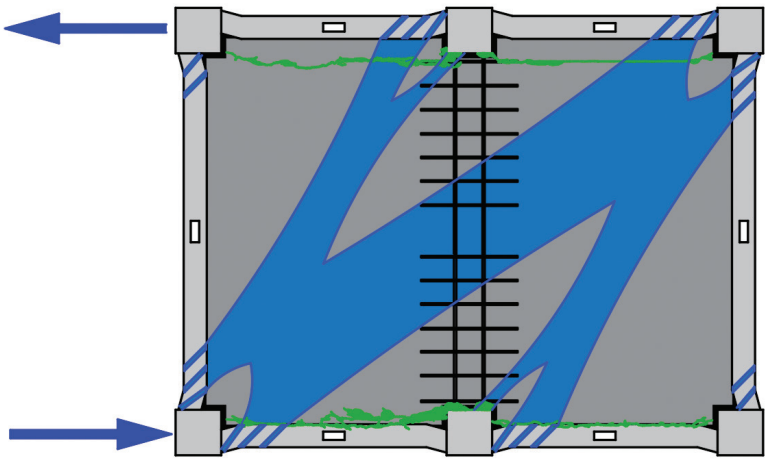

(a) Load-path with only compression struts displayed

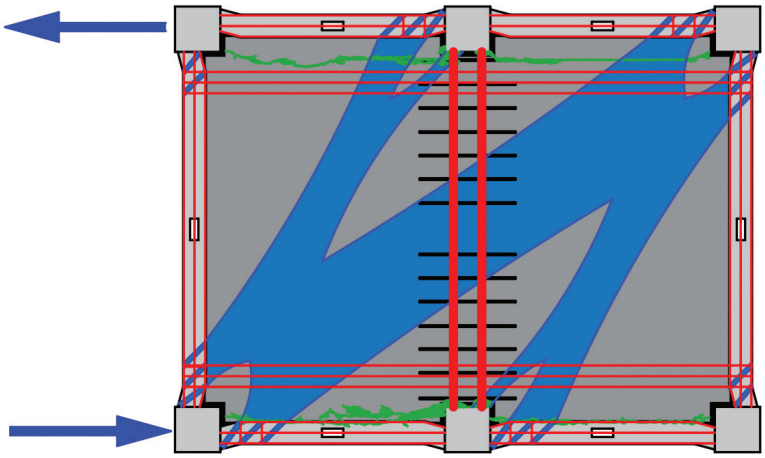

(b) Load-path with struts and tension ties displayed

Figure 23: TEST 2 Residual diagonal compression strut load-path under positive shear distortion loading

with approximately 20 mm vertical offset. Note that the critical crack along the southern end of the floor units traced a sinusoidal curve as shown in Figure 10 (a) that created clear compressive binding when shear distortion demands were applied.

The specimen diaphragm load-path at the initiation of the rhomboid #4 loading protocol is displayed in Figure 25 (a). At the northern end of the units the compressive struts could not land in the support beam A2B2 and B2C2 due to the very wide crack at the beam-to-unit interface. This meant the horizontal component of the strut force instead had to be tied back into the northern plastic hinge of beam C1C2 as shown in Figure 25 (a). The tie force in tie 2 of Figure 25 (a) was greatly increased compared to the regular force sustained in tie 1, as it collected force from the struts that could not land in the support beams moving west. The critical weak unit-to-unit interface, where most forces from the compression struts had accumulated within tie 2, was between unit 5 and unit 6, directly on the west side of the beta-beta unit stitching bar retrofit. At approximately 0.25% positive shear distortion of the floorplate, the tie force in tie 2 exceeded the mesh capacity, leading to mesh rupture at the north end of the unit 5 to unit 6 interface which then unzipped approximately 2/3rds of the mesh along the interface running southward. This led to the cracking displayed in Figure 25 (b) with the width of the north end of the crack being approximately 7 mm and the width of the south end of the crack being approximately 3 mm. Therefore, the loss of compression strut load-paths from the floor units into the northern beams explains why there was significantly more damage at the north end of the unit 5

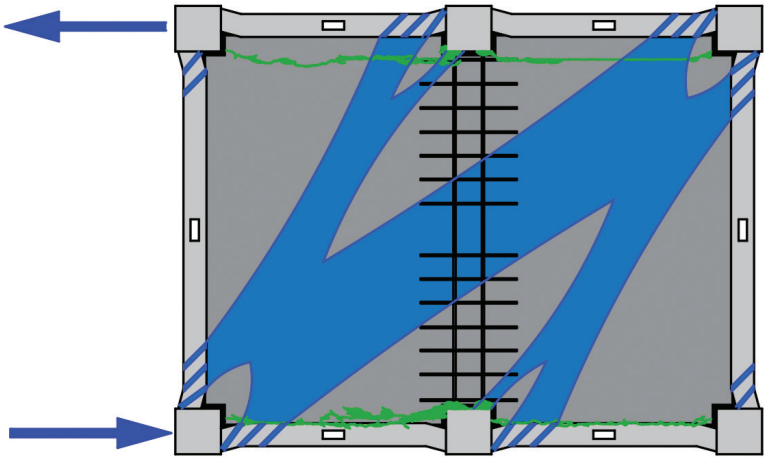

(a) Load-path with only compression struts displayed

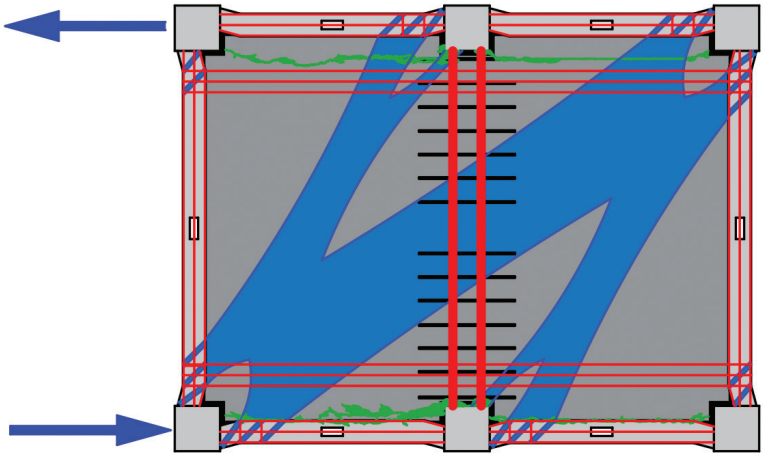

(b) Load-path with struts and tension ties displayed

Figure 24: TEST 2 Residual diagonal compression strut load-path under positive shear distortion loading

to unit 6 split in a system that was otherwise symmetrical. The crack caused an instant loss of plan shear stiffness and capacity under positive shear distortion as displayed in Figure 9 (b), with a drop in plan shear capacity of 100 kN (down to 580 kN from 680 kN) and an increase in shear distortion of 0.03% (up to 0.28% from 0.25%).

Interestingly, the loss of plan shear stiffness under positive shear distortion demands (following the unit 5 to unit 6 split occurring) was not observed when the floorplate was subjected to negative shear distortion demands. The reason for this becomes apparent when observing the different load-paths available between positive and negative plan shear distortion as shown in Figure 25 (b) and (c).

Under positive shear distortion, the split mesh between unit 5 and unit 6 meant a strut could not form from the floor to the intermediate column B2 near the tie bar anchor rubble. This meant tie forces needed to develop to link the strut and tie system back to where there was ability to cross the unit 5 to unit 6 split at the south end where the crack was not as wide and mesh was still intact. The contribution to plan shear stiffness from the western bay was greatly weakened by this.

Under negative shear distortion, while the inter-bay strut visible in Figure 25 (a) was still destroyed, the primary strut of the western bay could still form directly to the intermediate column B1 and the support beam B1C1 across the thinner end of the unit 5 to unit 6 split as shown in Figure 25 (c). This meant the plan shear stiffness and capacity was generally unaffected by the split under negative shear distortion, as the eastern bay primary strut was also unaffected by the unit 5 to unit 6 split.

The unit 5 to unit 6 split also greatly reduced the east-west bowstring effect following the rhomboid #4 loading protocol, as approximately 2/3rds of the tension ties linking the longitudinal beams were eliminated.

With the destruction of the north-south bowstring effect near the start of TEST 2 the longitudinal beams A1A2 and C1C2 had no restraint against beam elongation. This led to significant beam elongation throughout the test, reaching a maximum of approximately 30 mm elongation per plastic hinge by the end of the test following 5% drift demands as shown in Figure 26 (a). A similar effect of weakened bowstring effect restraint observed in TEST 1 was also observed for the surviving east-west bowstring effect in TEST 2, with the support beams only displaying slightly less elongation with respect to drift compared to the longitudinal beams as shown in Figure 26. Note that the red and orange dots in Figure 26, Figure 27 and Figure 28 all relate to the same points where bowstring effect actions were eliminated in the north-south direction (red) and severely weakened in the east-west direction (orange).

The cause of the reduction in the east-west bowstring effect beam elongation restraint is again evident when observing the torsional rotation of the beams that the floor tension ties of the bowstring were anchored into. Longitudinal beam A1A2 rotated into the floor-span with permanent deformation as displayed in Figure 27 (a), relieving tension forces in the east-west bowstring tension ties. The direct correlation between total elongation of the support beams A1B1 and B1C1 and plastic inward torsional rotation of the longitudinal beam A1A2 from the engaged east-west bowstring effect is displayed in Figure 28.

Note that the torsional rotation of support beams A1B1 and B1C1 was greatly reduced in TEST 2 as shown in Figure 27 (b) and (c) due to the elimination of the north-south bowstring effect at the start of the test. This is one of the primary drivers for the improved plan shear stiffness observed in TEST 2 at moderate to design level drift demands. Diaphragm compression struts were able to cross the wide cracks at the ends of the hollow-core units to link the frames, but tension ties were not. This meant the bowstring effect was not able to exceed the torsional capacity of the beams through the starter bars and therefore weaken the diaphragm diagonal strut load-path by reducing the capacity of the critical link of the beams in shear about their weak axes. Improved roughening of the beam-column casting joint in TEST 2 also likely had a positive effect on the torsional capacity of the beams compared to TEST 1, particularly at low drift and damage levels.

The unit 5 to unit 6 split and the weakening of the east-west bowstring effect it caused had a clear impact on the torsional rotation of longitudinal beam A1A2. Following the significant damage to the east-west bowstring effect, the rate of torsional rotation in A1A2 significantly decreased. This provides further evidence that the bowstring effect is the primary driver of beam plastic hinge torsional damage when applied simultaneously with major axis bending demands and therefore it is the primary driver of diaphragm shear stiffness degradation at moderate to design level drift demands.

Again, note that inward rotation in Figure 28 describes the top of the beams (where they are connected to the floor via starter bars) moving inwardly towards the floorplate. A visual representation of this and the starter bar demands that cause it is portrayed in Figure 16 (e).

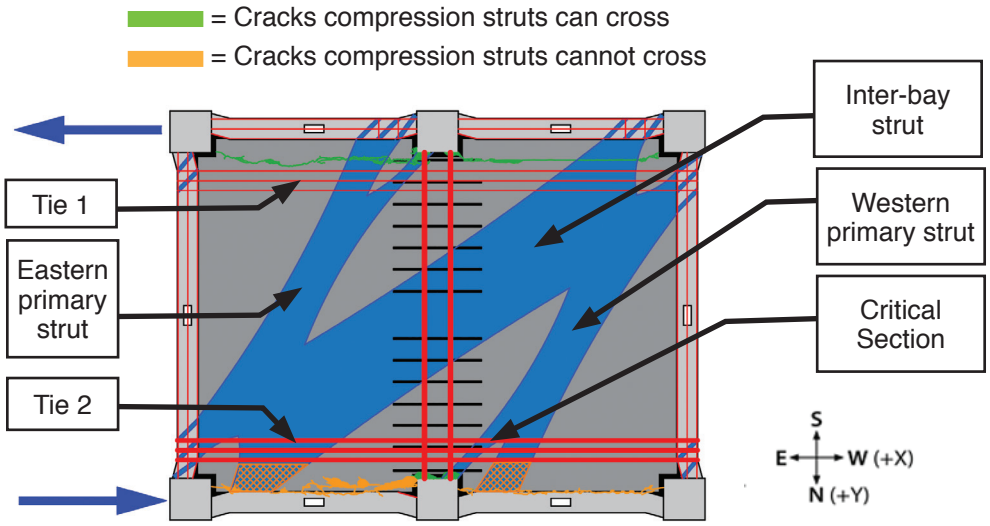

(a) Diagonal compression strut load-path at beginning of rhomboid #4

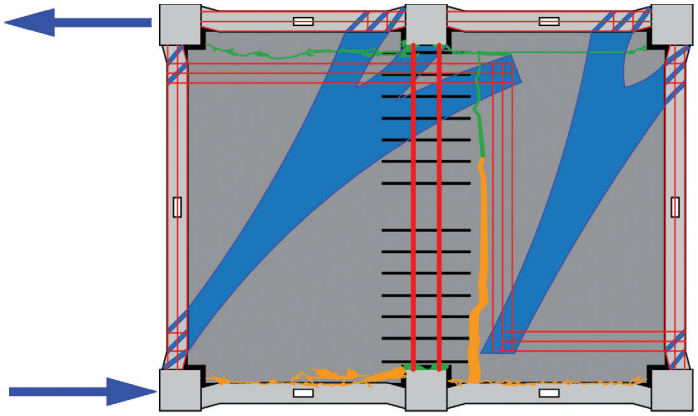

(b) Residual load-path after unit 5-unit 6 split under positive distortion demands

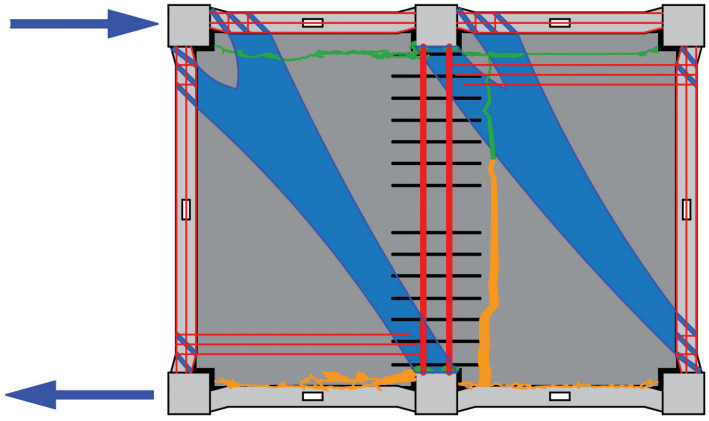

(c) Residual load-path after unit 5-unit 6 split under negative distortion demands

Figure 25: Tie force build-up leading to split between unit 5 and unit 6 during rhomboid #4 loading protocol

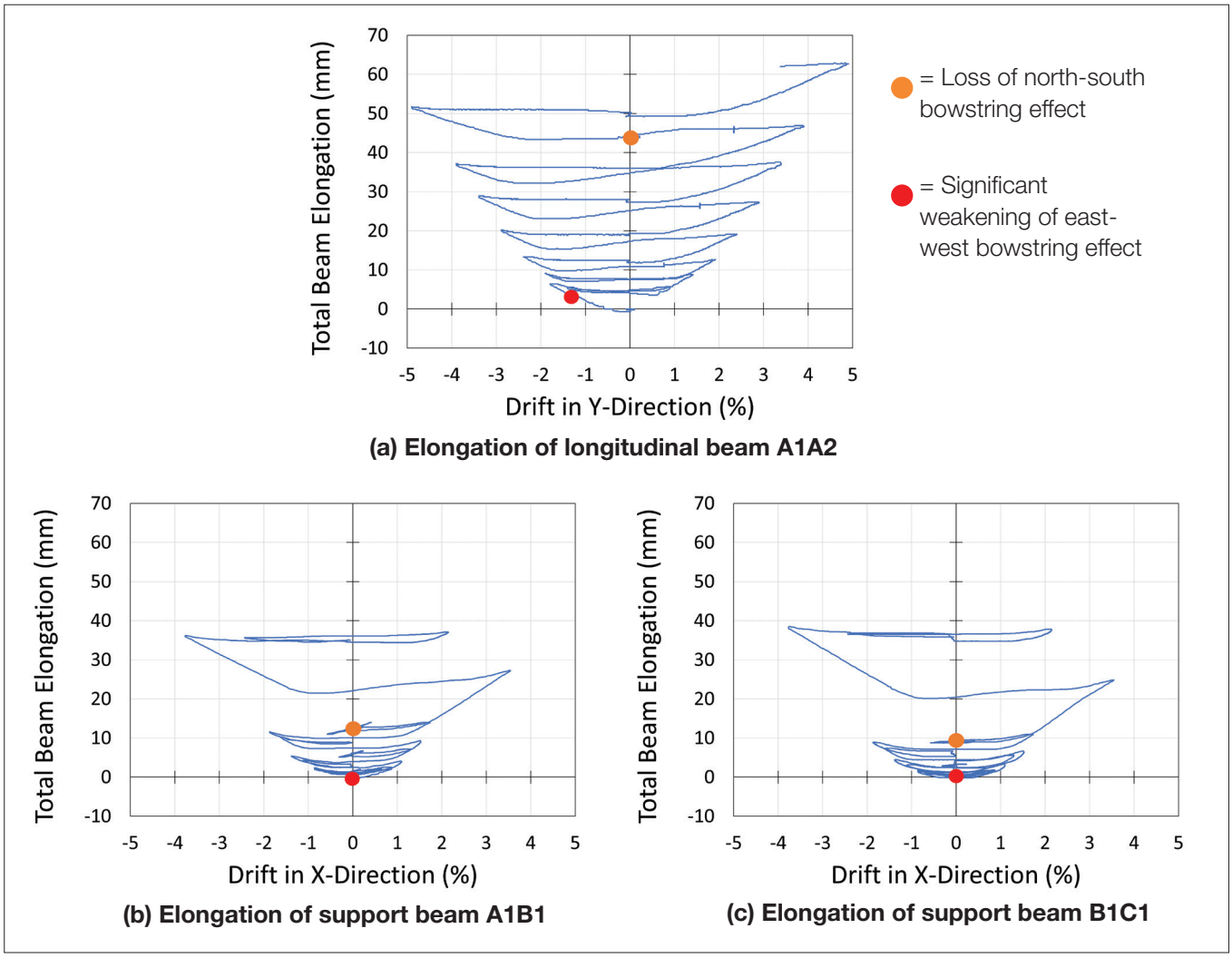

Figure 26: TEST 2 Elongation of support and longitudinal beams relative to their critical loading direction

3 CONCLUSIONS

The described analysis has led to the following conclusions and recommendations related to precast floor units and floor diaphragms:

3.1 QUALITATIVE DIAPHRAGM BEHAVIOUR CONCLUSIONS:

- Residual floor diaphragm load-paths will exist even at high damage states with very wide cracks if there is a viable gravity load path for the floor and there is adequate continuity reinforcement. However, there is high potential for the designed strut-and-tie load-paths to break down across beta-unit-to-beta-unit interfaces where precast flooring systems are used. Additionally, struts and ties can only reliably land in beams of the support frame and must be transferred into columns via the beam plastic hinge, rather than landing directly into columns. However, for column faces of intermediate columns where tie-bars were anchored, struts were observed landing into the column face only after large amounts of damage had occurred to the floor topping.
- Contact stresses form across wide concrete cracks in floors due to rubble replenishment (a process of aggregate rubble forming and falling into the gap as the crack interfaces become more damaged). These contact stresses provide a stiff connection resistant to plan shear deformation that can allow diaphragm compressive struts to land on beams. Rubble formation appears to primarily initiate near

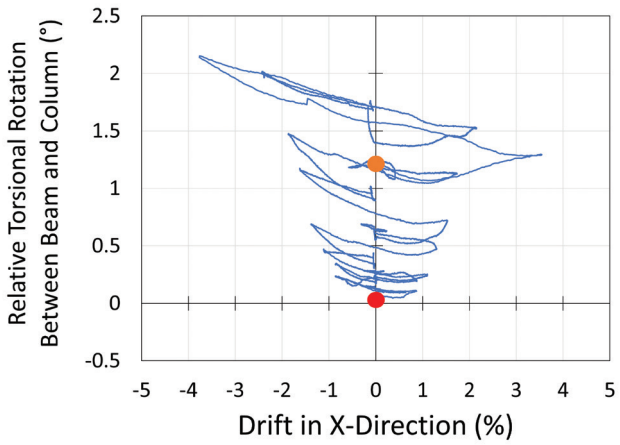

(a) Torsional rotation of longitudinal beam A1A2 relative to columns A1 and A2

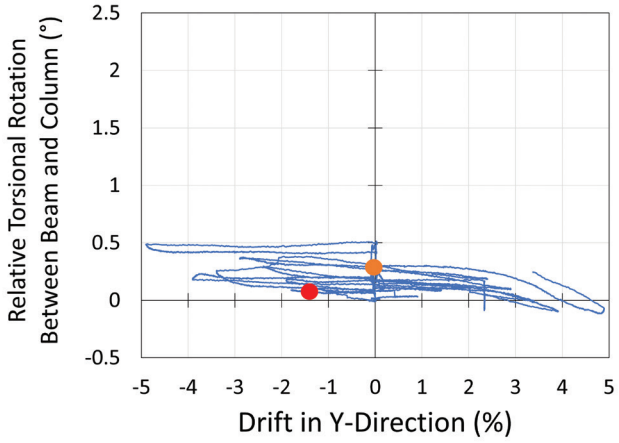

(a) Torsional rotation of support beam A1B1 relative to columns A1 and B1

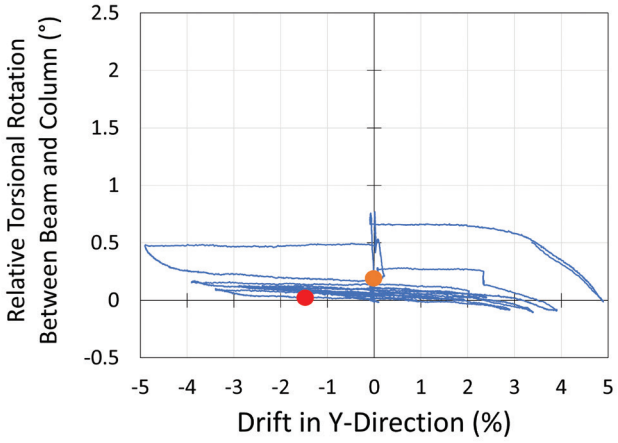

(b) Torsional rotation of support beam B1C1 relative to columns B1 and C1

Figure 27: TEST 2 Torsional rotation of support and longitudinal beams relative to their supporting columns

steel reinforcing, particularly deformed rebar. This is likely due to the bond with the bar causing substantial local cone-type cracking in the concrete when the more ductile bar deforms. Based on limited test data presented herein, starter bar spacing of 400 mm centre-to-centre crossing the crack interface appears to provide adequate rubble formation to transfer load across wide cracks. Smaller starter bar spacing should increase rubble formation, further ensuring a residual load path develops. It is proposed that the maximum reliable crack width a compression strut can form across is dependent on the aggregate size used in the topping concrete mix. This is because aggregate rubble is what wedges between the crack interfaces, and individual pieces of aggregate are unlikely to crush under compressive demands.

- The limiting factor determining floor diaphragm in-plane shear stiffness is the surrounding beam resistance to torsional deformation within their plastic hinges. Once the beams are torsionally overloaded due to a combination of elongation, simultaneous strong and weak axis bending and torsional moment, the frame beam elements become weaker and more flexible than the floor diaphragm elements. The primary driver of this damage mode (when simultaneously applied with other demands) is the bowstring effect.

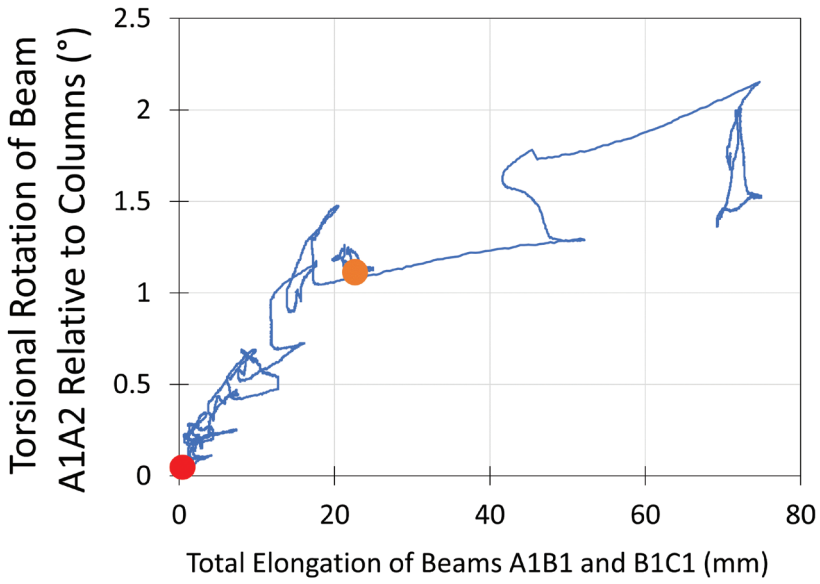

Figure 28: TEST 2 Inward rotation of longitudinal beam A1A2 driven by elongation of the orthogonal support beams A1B1 and B1C1

As tension ties in the floor resist beam elongation of beams in the orthogonal direction, these tie forces are applied to the critical beam through the starter bars which enforces significant torsional demands on the critical beam. This diaphragm degradation mechanism leads to a much lower diaphragm in-plane shear stiffness than the initial stiffness at moderate to design level drifts as displayed in Figure 12. This means the rigid diaphragm assumption may not be valid when modelling structural response under earthquake loading.

- Beam loss of torsional stiffness impacts the diaphragm stiffness because struts must pass through the beam in a weak-axis shear mode through the plastic hinge to reach columns. As the beam twists it may deform the interior bottom bars, cracking the surrounding concrete and reducing their confinement and bond with the rest of the beam. This decreases their contribution to dowel action with an unsupported length to resist shear determined by the stirrup spacing, which is a much weaker and less stiff contribution to the beam shear load path. Additionally, twisting of the beam across the primary crack near the beam-column interface likely grinds the two sides of the crack smoother over multiple cycles, reducing aggregate interlock and the friction necessary to maintain the compressive portion of the weak axis shear load-path.
- A positive of the beam torsional softening effect for hollow-core floor systems is that it may mitigate, to some extent, undesirable local failure modes such as negative moment and positive moment failure of individual floor units. This is because the deformation incompatibility demands are capped at this point as the support beam deforms plastically about its torsional twisting axis. The negative of this effect is the differential twisting of support and longitudinal beams which heavily damages the ends of alpha units (hollow-core end units positioned next to longitudinal beam) in the floorplate corners.
- Test data indicates that the diaphragm can lose as much as 75% of initial stiffness after drift demands exceed approximately 1% (in an earthquake with a directionality ratio of 1:1). In an earthquake with a directionality ratio of 1:2 (Test 2), stiffness can degrade 50% by 1.5% drift. As support frame beam elements lose torsional stiffness, load sharing between columns via floor diaphragm in-plane shear (or compression

struts) decreases. This leads to a more flexible structural response as the rigid diaphragm assumption becomes less accurate as damage progresses. The impact of this would differ depending on the structural layout and ground motion with respect to whether this amplifies or damps the structural response at moderate damage levels. Further experimental research, preferably using shake tables to provide inertial and damping response, would be required to quantify this effect.

- Directionality of earthquake loading plays a large role in determining the rate that in-plane stiffness contribution from a floor diaphragm degrades. The closer an earthquake record is to exhibiting equal displacement demands in all directions (i.e. circular bidirectional loading pattern), the earlier the diaphragm in-plane shear stiffness will degrade. This is because larger amounts of simultaneous action overpower the beam plastic hinge capacity earlier, by introducing larger weak axis bending and torsional demands while the longitudinal bar capacity is being used for strong axis bending. The converse is that the closer an earthquake is to being unidirectional (and in the direction of one of the primary frame axes of the building), the higher peak demands the supporting beams can withstand before losing torsional stiffness and therefore, the longer the floor diaphragm will remain stiff in-plane against shear deformation. This type of pulse demand would be expected in near-fault earthquakes. The downside of the stiffer diaphragm under these loading conditions is that higher deformation incompatibility demands are imparted into the floor units, making for a worse case for undesirable failure modes in hollow-core such as positive and negative moment failure modes as described in (Büker et al. 2022).
- Tie-bars are currently required between intermediate columns (with tie capacity to exceed 5% of maximum total axial compression force acting on the linked column or exceed 20% of the shear force from seismic actions in the column: Cl. 10.3.6 of NZS 3101:2006) to prevent them from bowing out of the structure which can lead to catastrophic floor failure. A secondary benefit of tie bars was observed during testing; that rubble is generated near the tie-bar anchor locations under earthquake loading due to bond stresses between the tie-bar and floor topping. However, this residual contact stress load path associated with the concrete around the column tie bars appears to require extensive diaphragm damage and is only likely to develop after the building has experienced high peak drifts.
- The interface between beta units is a critical weak point in diaphragm load-paths. This is because of deformation incompatibility between the units as the plastic hinges they are seated on undergo strong axis bending during earthquake loading, meaning the critical loading direction is orthogonal to the hollow-core unit layout. This causes one beta unit's elevation to rise and the other to fall along the beta-beta unit interface which leads to very early cracking and early rupture of the mesh along it. Additionally, this is the weak section of the bowstring effect action linking longitudinal beams, placing all mesh across the beta-beta unit interface in tension and providing further demands on the mesh across the beta-beta unit interface leading to early rupture. Being the weak section for the bowstring effect makes the beta-beta unit interface critical in determining the diaphragm performance of the floorplate. It is noted that once this connection between beta units is severed, the rate of beam elongation and degradation of beam torsional stiffness greatly accelerates in both primary frame directions.

3.2 RECOMMENDATIONS FOR PRACTITIONERS

- The findings from two super-assembly experiments provided a quantitative relationship between a structure's previously experienced drift demand (magnitude and directionality) to the degradation of diaphragm shear stiffness. In the future it would be beneficial for more experimental testing using rhomboid loading protocols to provide further data; however, as the frame and floor section sizes and steel detailing used in the two experiments were typical of mid-rise reinforced concrete buildings, the generalised Equations (7) and (8) are a useful preliminary tool to estimate diaphragm shear stiffness degradation.

  This relationship shows that diaphragm shear stiffness losses following typical ultimate limit state drift demands of 2.5% range from approximately 80% to 95% of the initial stiffness depending on earthquake directionality. Further explanation of the development of Equations (7) and (8) are shown in Section 2.1.
- In TEST 2 a retrofit referred to as "stitching bars" was used to strengthen the beta-beta unit interface. This retrofit greatly improved both the local hollow-core stability as well as maintaining the diaphragm load-path and bowstring effect across the two floor bays. It is therefore recommended that beta-unit-to-beta-unit stitching bars are added to tie-bar configurations. Even though failure of the units is delayed with the stitching bars, that failure is eventually shifted from the unit-to-unit interface to the end of the stitched

bars. To avoid failure through the unit as observed in TEST 2, it is recommended that the stitched bars be extended the full width of each beta unit. These should be deformed bars, and as an interim recommendation the strength and spacing of the stitching bars should be one sixth of the force of the tie bars (combined), at spacings equal to one third of the development length of the tie bars and these stitching bars are to be provided along the full length of the ties at this size and spacing. This ensures there is adequate strength to maintain the tension tie load-path across the beta-unit-to-beta-unit interface, removing it as a critical weak zone.

- The best way to ensure that diaphragm residual compressive strut forces can reach their landing points on beams is to provide adequate seating for the floor elements regardless of the floor system typology. In the case of hollow-core systems, seating recommendations are provided in (MBIE, et al2018) and recommendations for seating angle retrofits to improve seating lengths are provided in Büker et al. 2022. If there is a viable gravity load-path for the floor elements near the beam-floor interface, cracks that form in the floor will allow diaphragm compressive load-paths across the cracks through the rubble replenishment phenomenon observed in TEST 2 and described in Section 2.1.
- It is proposed that only column faces with tie-bar anchor points installed may be used as compression nodes in strut-and-tie analysis. This is due to the formation of rubble aggregate in the floor topping caused by deformation incompatibility demands with the tie-bars. This rubble aggregate can jam between the floor-to-column interface, bridging gaps that develop due to beam elongation.

4 REFERENCES

Angel, N., Correal, J., and Restrepo, J. (2019). "Cyclic Behaviour of Hollow-Core Diaphragm Subassemblies." PCI Journal, March-April 2019, 80-96.

Brooke, N. (2022). "Overview of Retrofit Requirements and Techniques for Precast Concrete Floors." SESOC Journal, 35(1).

Büker, F., Hogan, L., Brooke, N., Elwood, K., and Bull, D. (2022). "Design Recommendations for Seating Angles." SESOC Journal, 35(1).

Büker, F., Parr, M., De Francesco, G., Hogan, L., Bull, D., Elwood, K., Liu, A., and Sullivan, T. (2022). "Seismic Damage Observations of Precast Hollow-Core Floors From Two Full-Scale Super-Assembly Tests." SESOC Journal, 35(1).

MBIE, EQC, NZSEE, SESOC, and NZGS. 2018. Technical Proposal to Revise the Engineering Assessment Guidelines - Part C5 Concrete Buildings. Wellington, New Zealand: Ministry of Business, Innovation, and Employment.

Lindsay, R. (2004). "Experiments on the Seismic Performance of Hollow-Core Floor Systems in Precast Concrete Buildings." MEng, University of Canterbury, Christchurch, New Zealand.

MacPherson, C. (2005). "Seismic Performance and Forensic Analysis of a Precast Concrete Hollow-Core Floor Super-Assemblage." M.Eng, University of Canterbury, Christchurch, New Zealand.

Nievas, C., and Sullivan, T. (2017). "Accounting for Directionality as a Function of Structural Typology in Performance-Based Earthquake Engineering Design." Earthquake Engineering and Structural Dynamics, 46, 791-809.

Parr, M. (2022). "Retrofit Solutions for New Zealand Hollow-Core Floors and Investigation of True Floor Diaphragm Load Paths in Earthquakes." PhD, University of Canterbury, Christchurch, New Zealand - Currently in preparation.

Parr, M., Büker, F., De Francesco, G., Bull, D., Elwood, K., Hogan, L., Brooke, N., Liu, A., and Sullivan, T. (2022). "Load-Path and Stiffness Degradation of Floor Diaphragms in Reinforced Concrete Buildings Subjected to Lateral Loading – Part I, Experimental Observations." SESOC Journal, 35(1).

Paulay, T. (1996). "Seismic Design of Concrete Structures - The Present Needs of Societies." Eleventh World Conference on Earthquake EngineeringAcapulco, Mexico.

Vecchio, F., and Collins, M. (1986). "The Modified Compression-Fielf Theory for Reinforced Concrete Elements Subjected to Shear." ACI Journal, 83-22(March-April 1986), 219-231.

ISSN No. 2744-7871